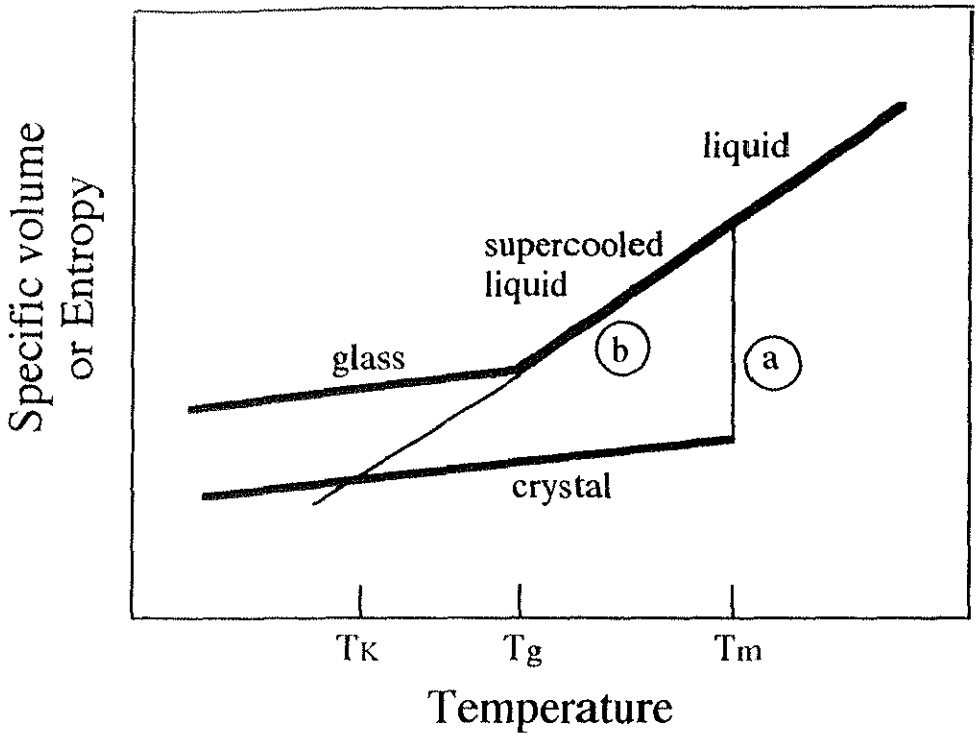

Fig. 1. 1 Cooling of a liquid leads the route of either crystallization (a) or forming a glassy state via supercooled liquid (b). T_m, T_g and T_K indicate the melting, glass transition and Kauzmann temperatures, respectively.

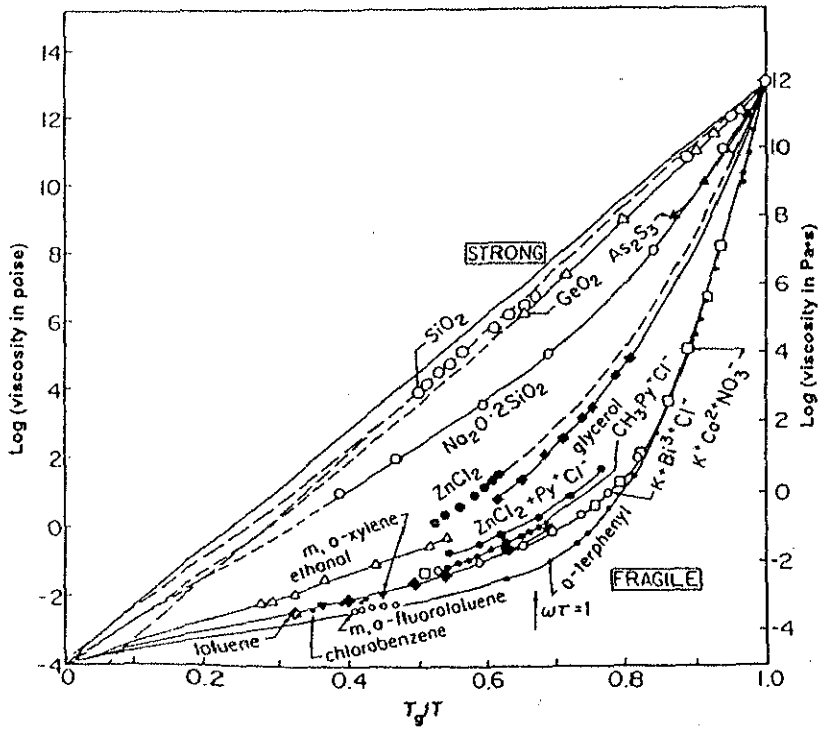

Fig. 1. 2 Classification of liquids: strong and fragile liquids. This classification is based on the viscosity data, $\log_{10}\eta$ vs normalized inverse temperature, T_g/T [2].

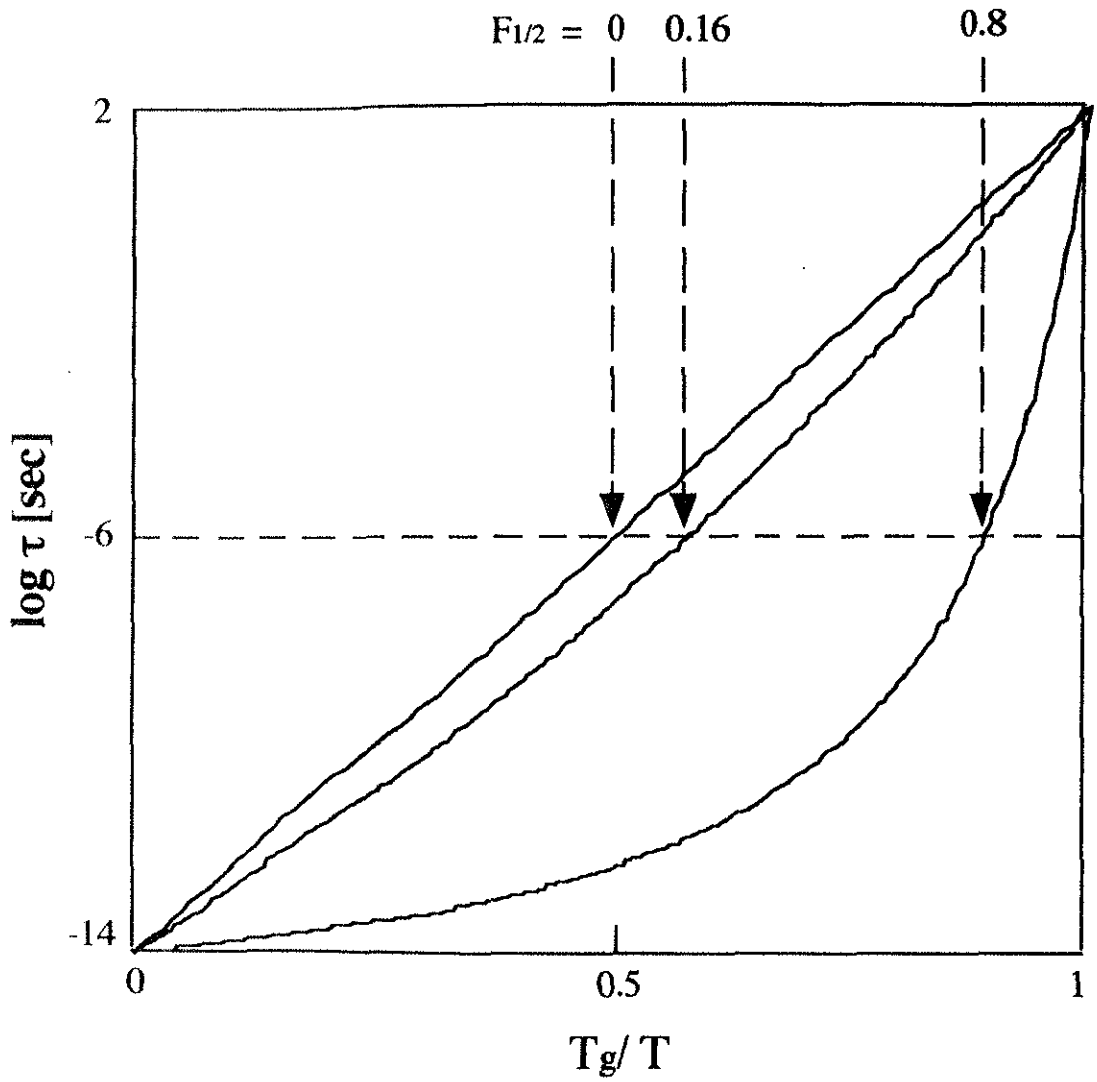

Fig. 1. 3 Definition of fragility, $F_{1/2}$. It is expressed in terms of relaxation time, $\log_{10}\tau$, vs normalized inverse temperature, T_g/T. $F_{1/2}$ = 0, 0.16 and 0.8 are shown as examples.

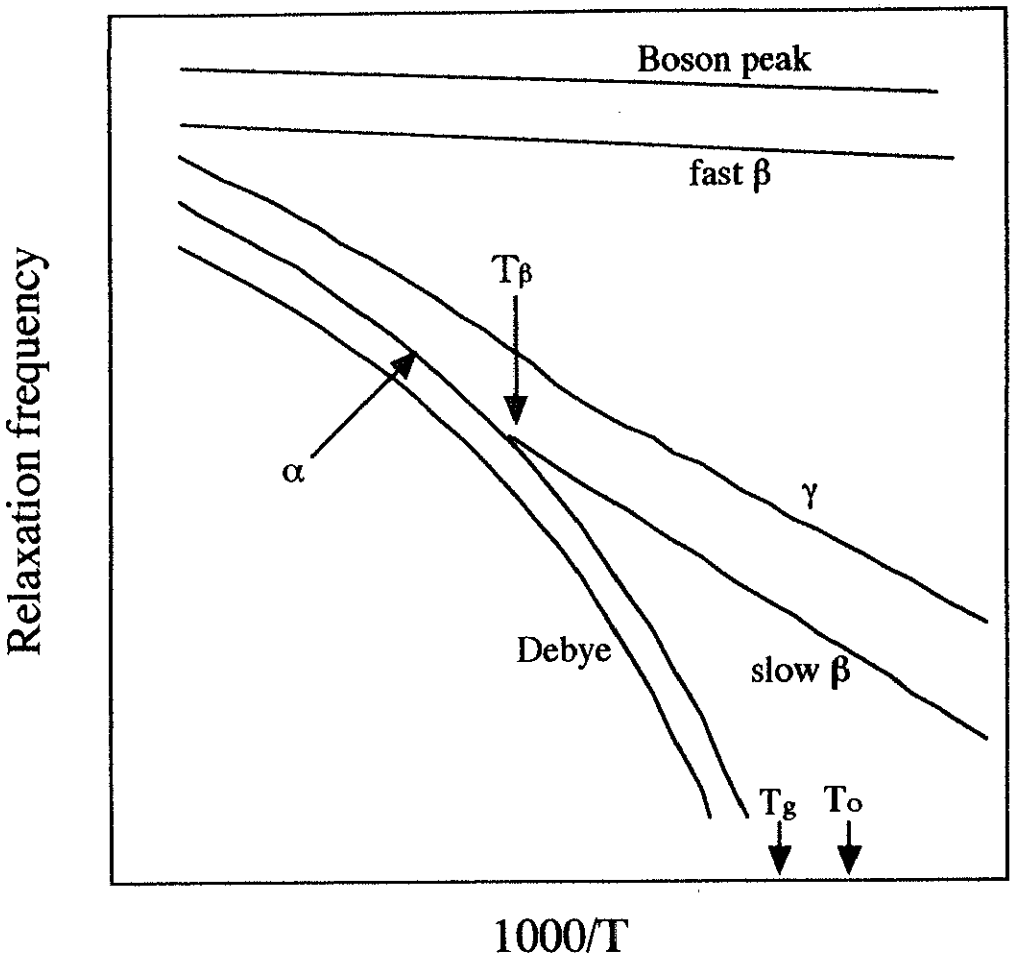

Fig. 1. 4 Several relaxation modes in liquid and glass states. The α relaxation is related to the glass transition. The slow β, γ and fast β relaxations and Boson peak are observed both above and below T_g and can be usually reproduced by the Arrhenius law, $f = f_{0A} \exp(-A/T)$. T_g and T_0 indicate glass transition and Vogel-Fulcher temperature in the VTF law, $f = f_{0B} \exp[-B/(T - T_0)]$, respectively.

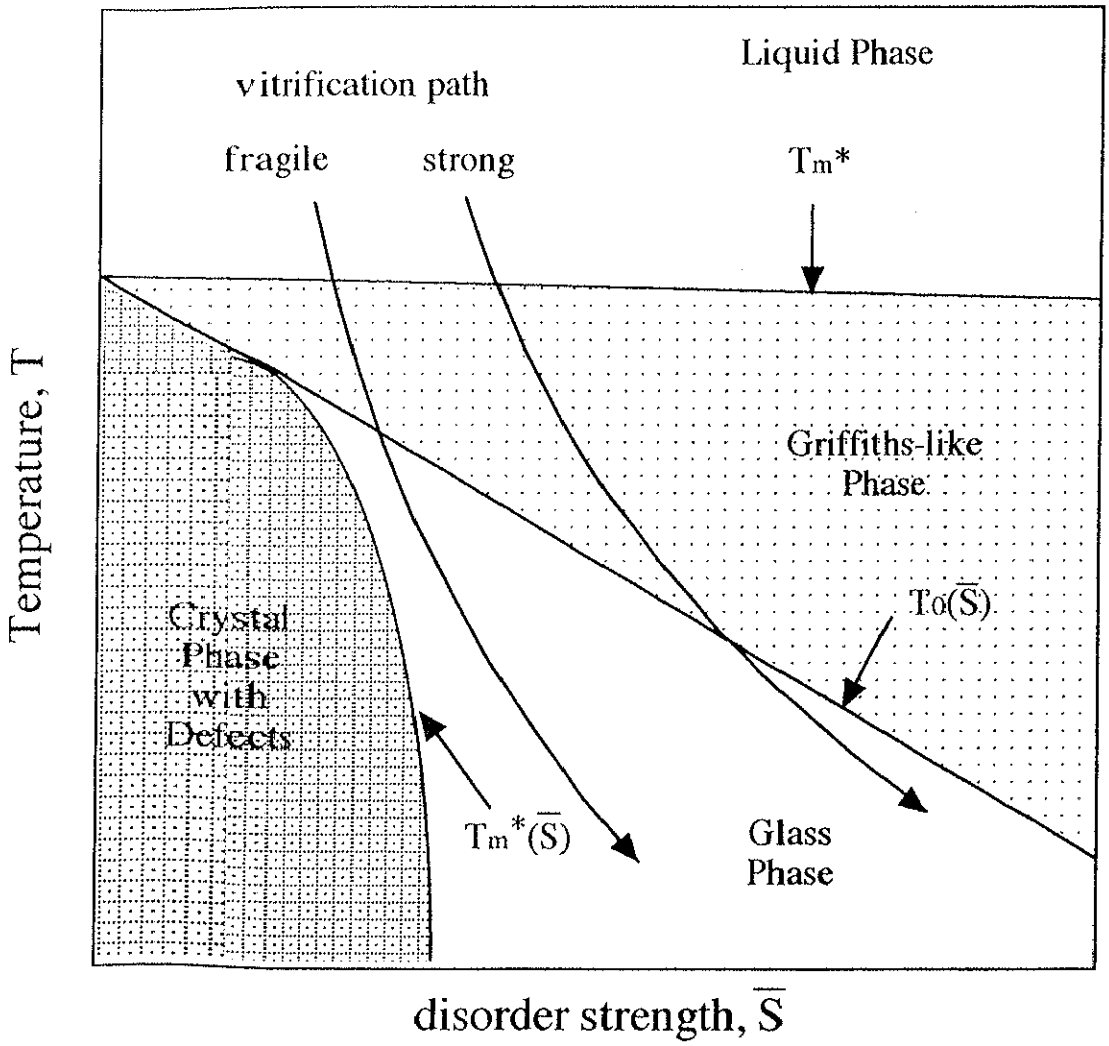

Fig. 2. 2 The vitrificaion path from liquid to glass phase. T_m^* and $T_m^*(\bar{S})$ represent the melting temperatures of extrapolated and crystal with defects, respectively. $T_o(\bar{S})$ is the ideal glass transition temperature, usually called Vogel-Fulcher temperature [11].

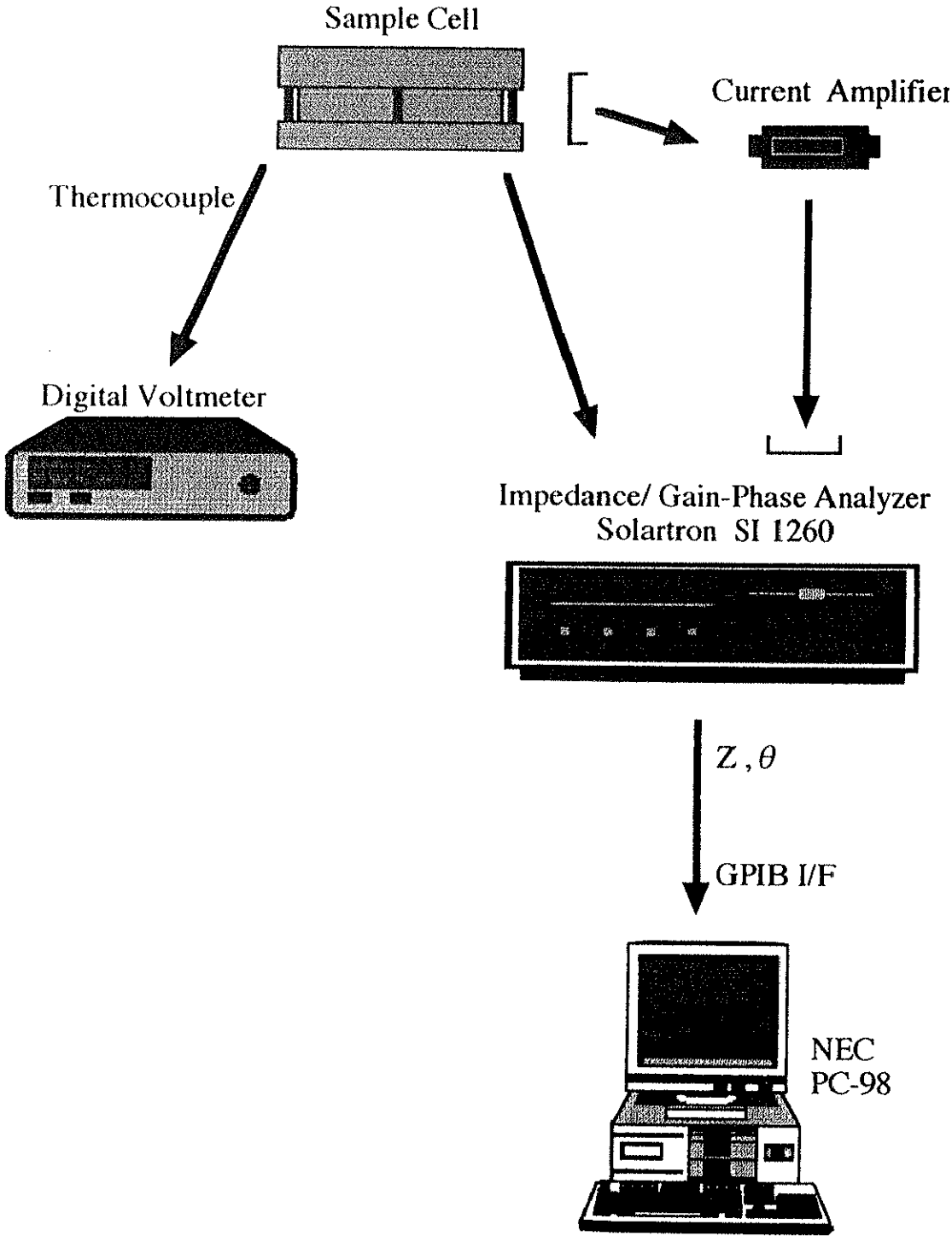

Fig. 3.1 Block diagram of Impedance Analyzer (IA) system

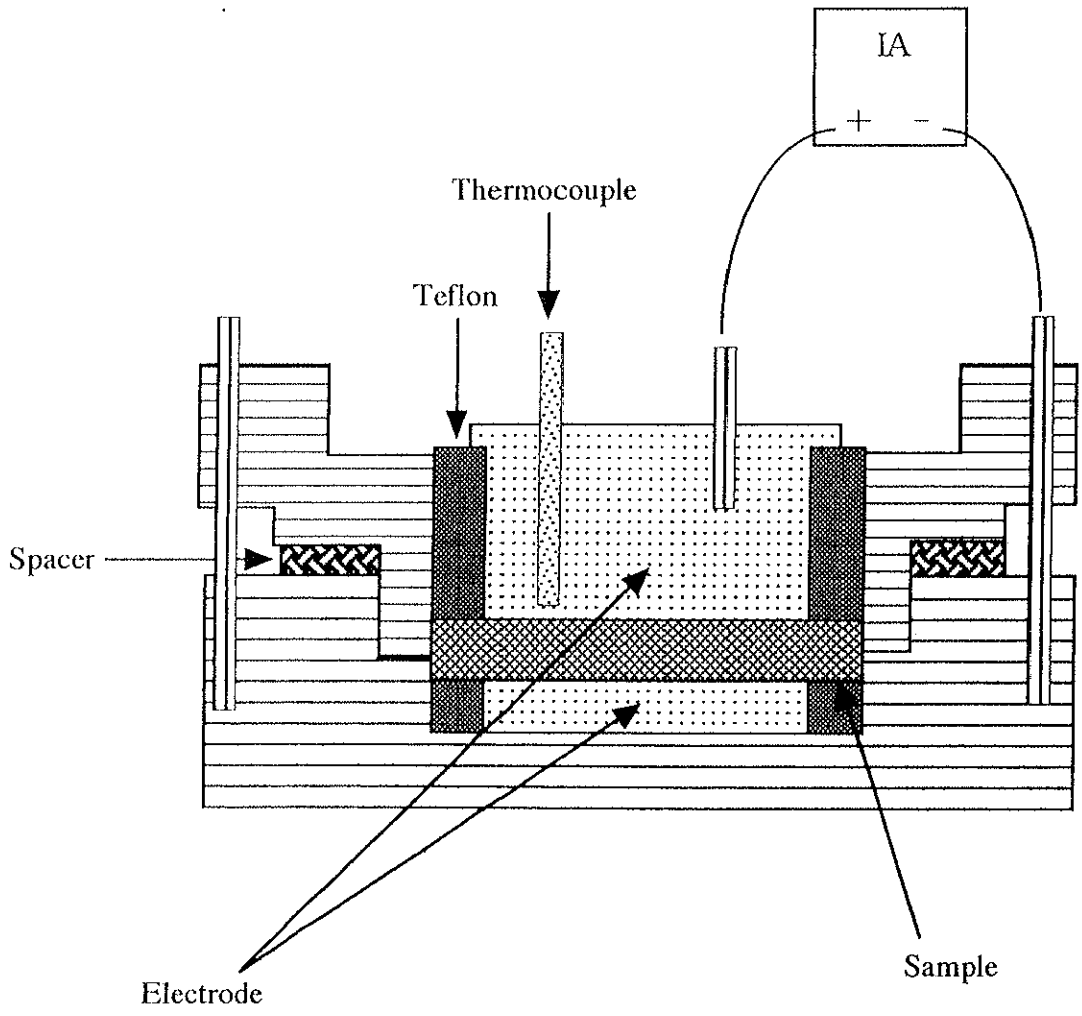

Fig. 3. 2 Cross-section of the sample cell used in IA system.

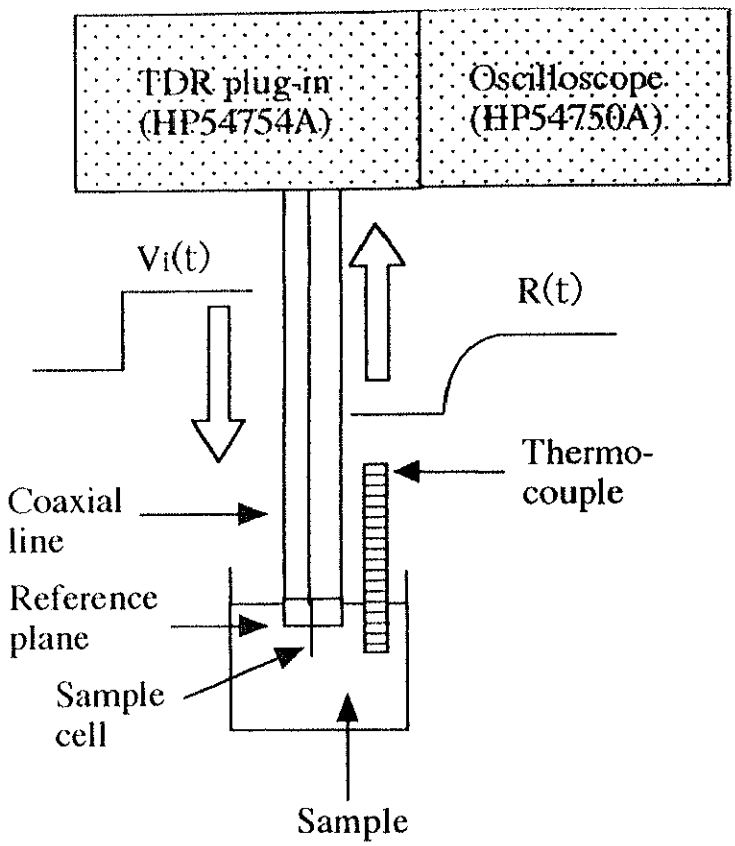

Fig. 3. 3 Schematic illustration of TDR system. Vi(t) is a step-like incident pulse and R(t) is the reflected pules from the sample. Vi(t) and R(t) propagate along the same coaxial line but in opposite direction..

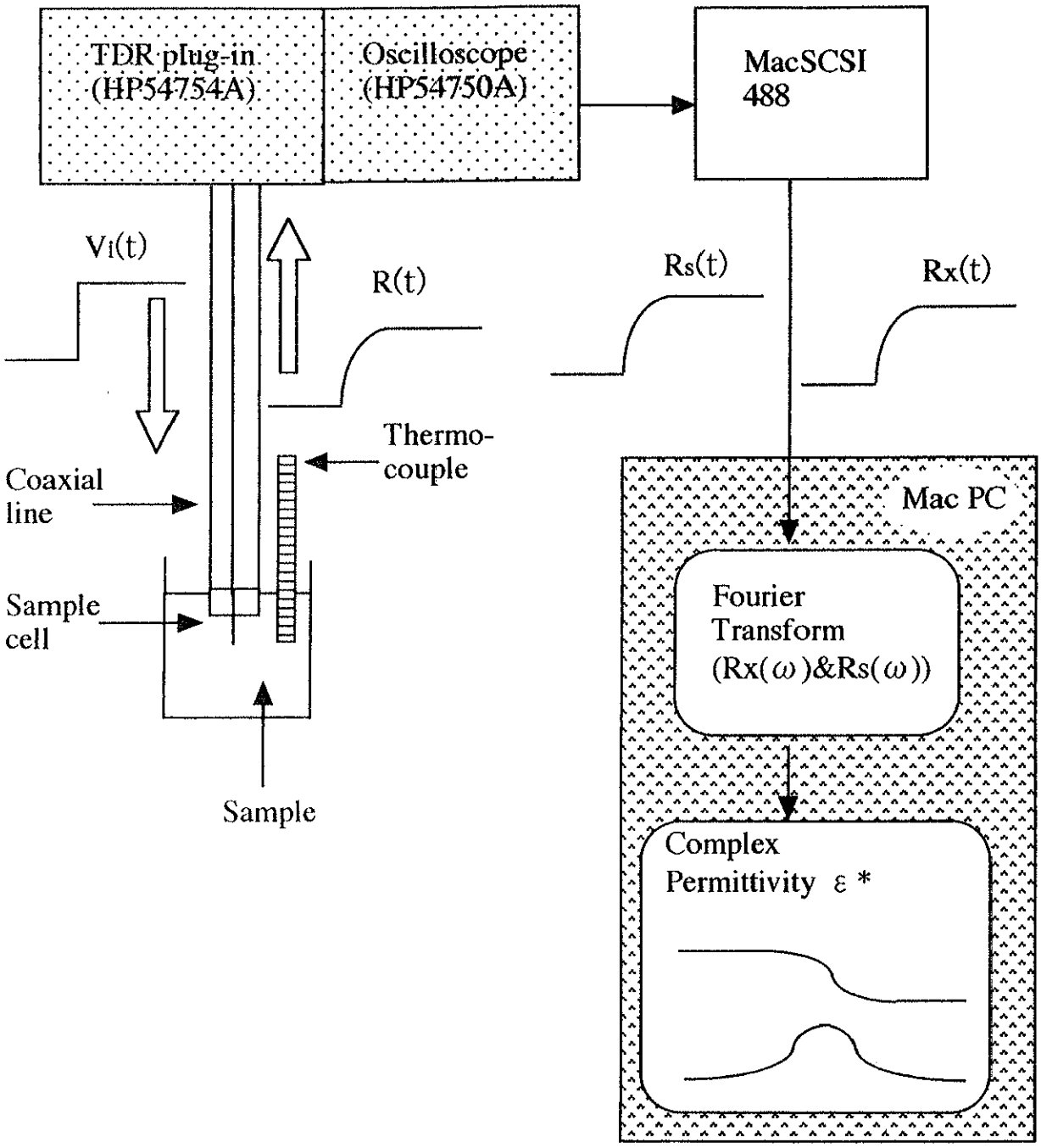

Fig. 3. 4 Block diagram of TDR system. Vi(t) and R(t) are the incident and reflected pulses. Rs(t) and Rx(t) are the reflected pulses from the standard and sample materials, respectively. The reflected pulses, Rs(t) and Rx(t), are saved in the oscilloscope, then transferred to the computer through MacSCSI488 bus controller and performed by the Fourier transform. Their corresponding Fourier transforms are Rs(ω) and Rx(ω). Air was used as a standard material.

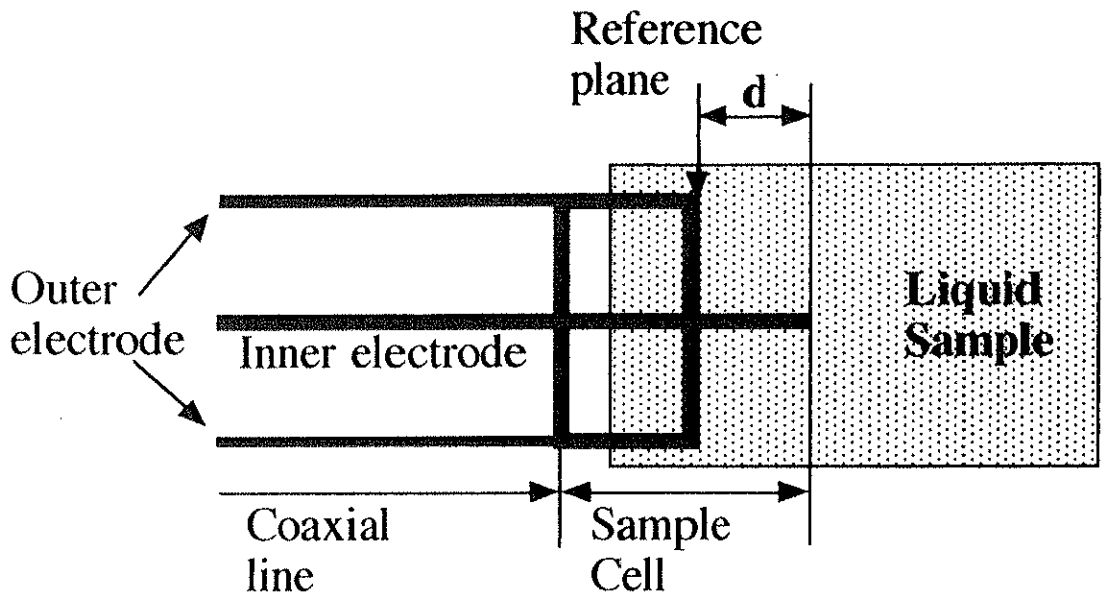

Fig. 3. 5 Sample cell composition of TDR system. Sample cell is based on the SMA connector and connected to coaxial line. The pin part of sample cell is fully dipped into the liquid sample.

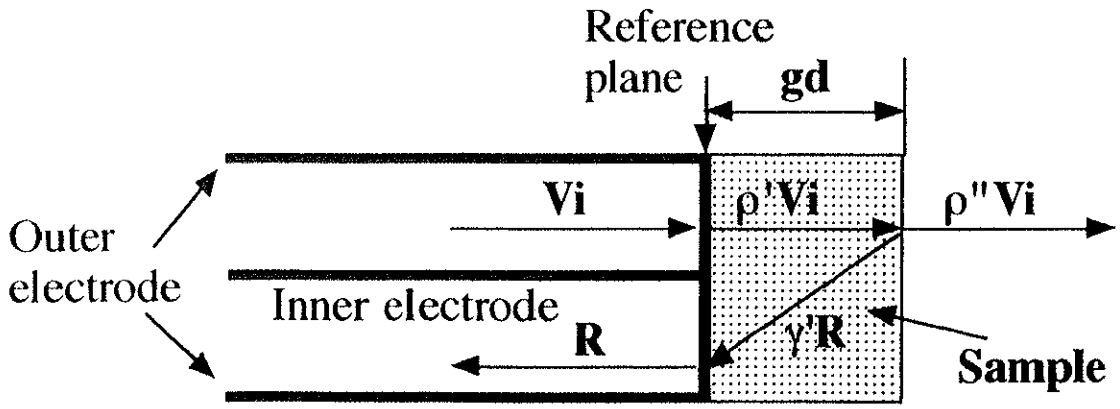

Fig. 3. 6 The simple and schematic transmission and reflection. Vi represents the incident pulse. It is considered that ρ' Vi transmits into the sample and γ' R reflected at the end plane of sample with the length of gd. R and ρ"Vi are the total reflected and transmitted pulses due to the presence of the sample.

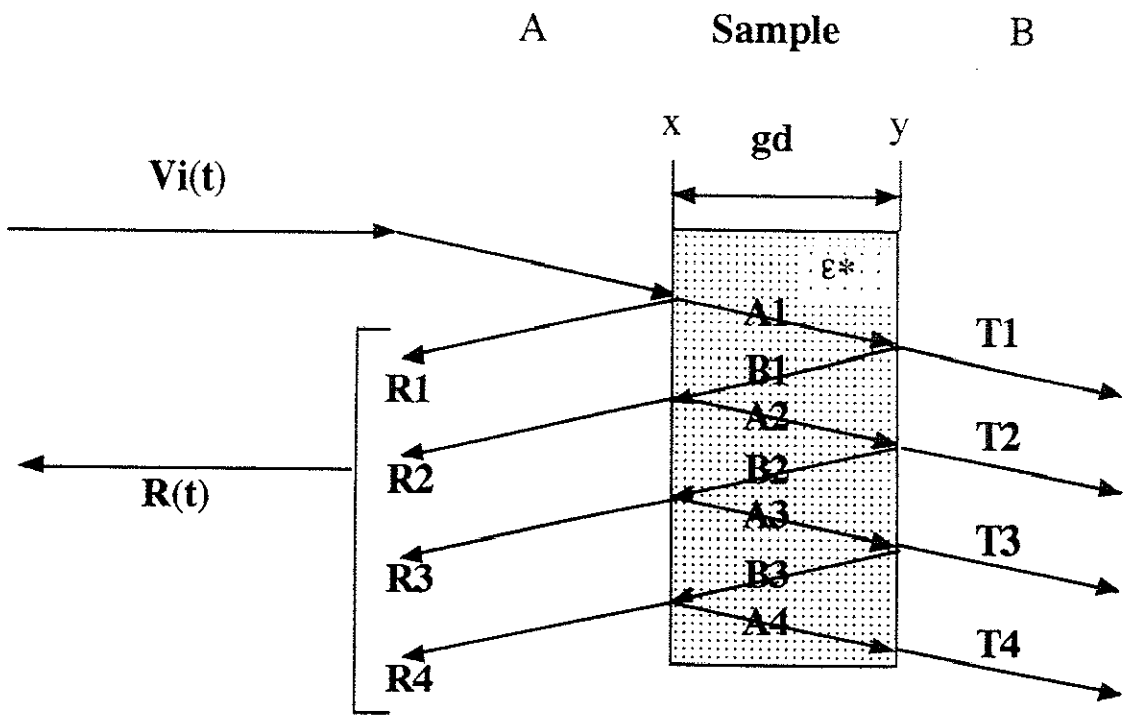

Fig. 3. 7 Multiple reflection and transmission from the sample with length gd and complex dielectric permittivity ε*. It is supposed that the sample is inserted between the materials A and B. The interfaces between sample and material A and B are represented as x and y planes, respectively. Vi (t) is the incident pulse. It occurs the reflection and transmission at plane x. R1 and A1 are the reflected and transmitted pulses at x plane. The transmitted A1 pulse is reflected and transmitted as B1 and T1 at y plane. The reflected B1 again transmitted into material A at x plane. It corresponds to R2. These reflection and transmission are repeated at x and y planes.

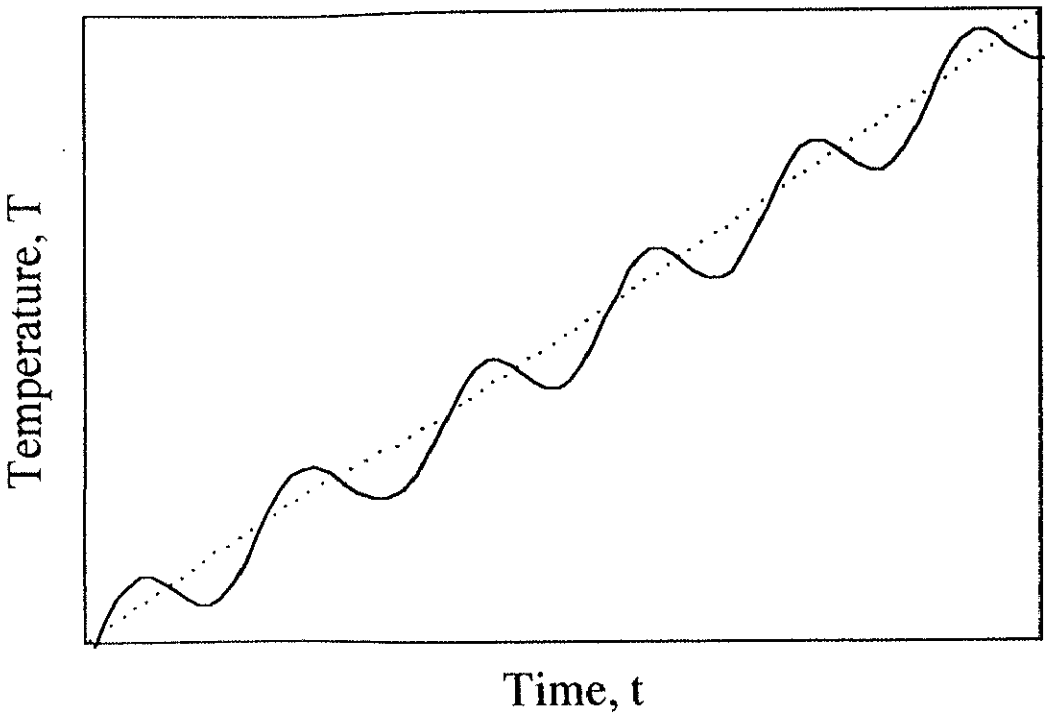

Fig. 3. 8 Temperature changes in both MDSC (solid) and conventional DSC (dotted). The temperature changes linearly in case of the conventional DSC, $T(t) = To + qt$. In case of MDSC, the sinusoidal temperature change is superposed to DSC, $T(t) = To + qt + A \sin(2\pi t/P)$

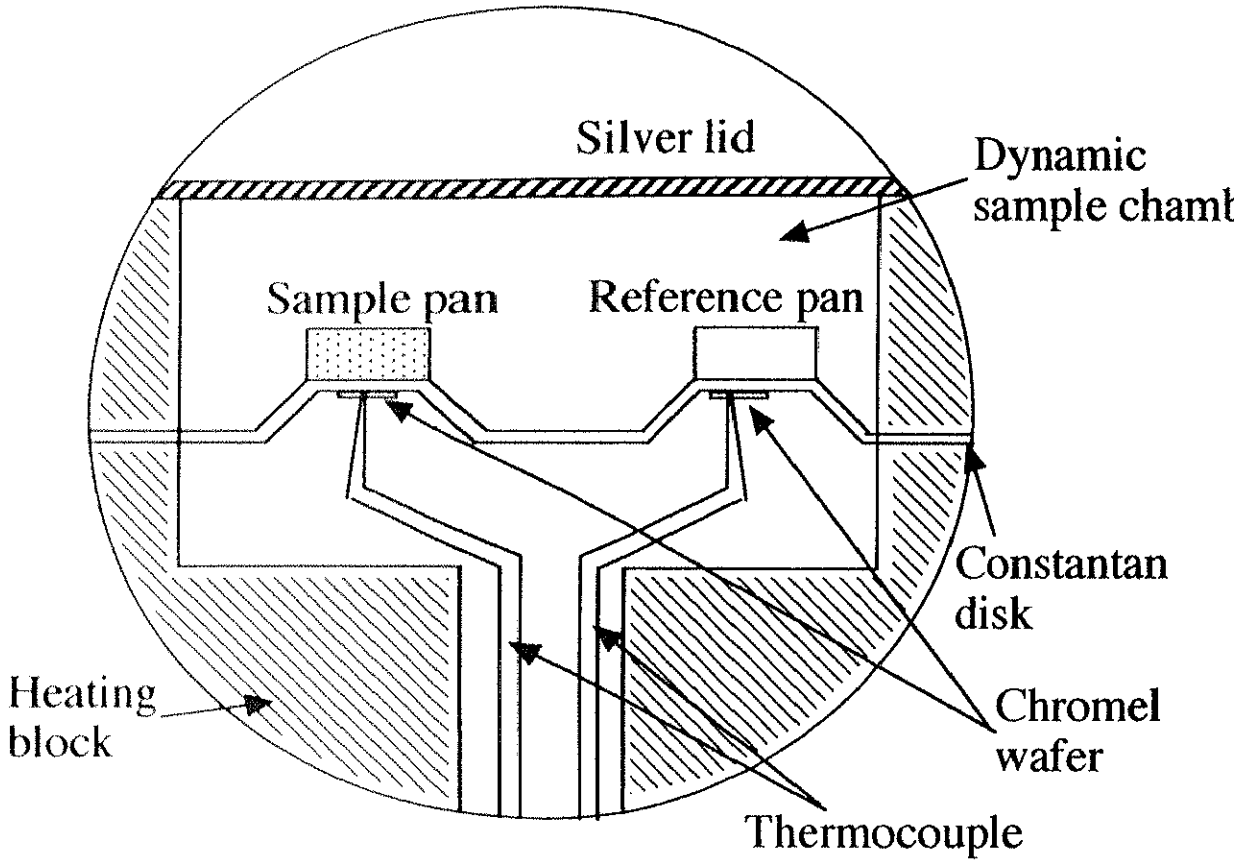

Fig. 3. 9 Cross section of DSC cell

1	nPrOH (n-propanol)	PG (propylene glycol)	Gly (glycerol)
	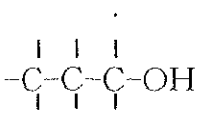	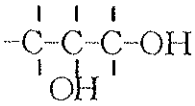	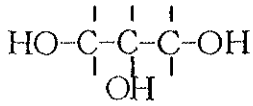
2	nPrOH	iPrOH (i-propanol)	
	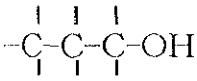	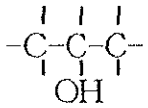	
3	nPrOH nPrOD (n-propanol-d1)	iPrOH iPrOD (i-propanol-d1)	
		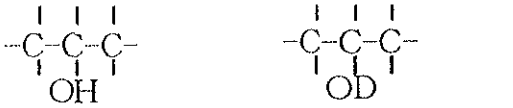	
4	PG PG Monomethyl Ether (PGME)	tPG tPGME	
	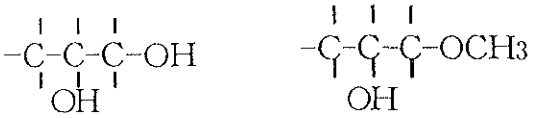	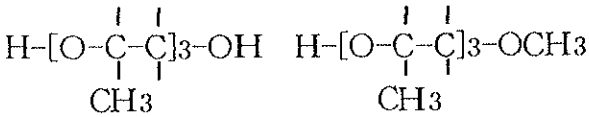	
5	PG (n=1), tPG (n=3), PPG425 (n=7), PPG725 (n=12), PPG2000 (n=34), PPG4000 (n=69)		
	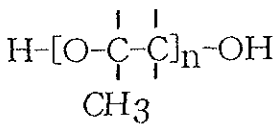		

Fig. 3. 10 Chemical structures of the materials studied.

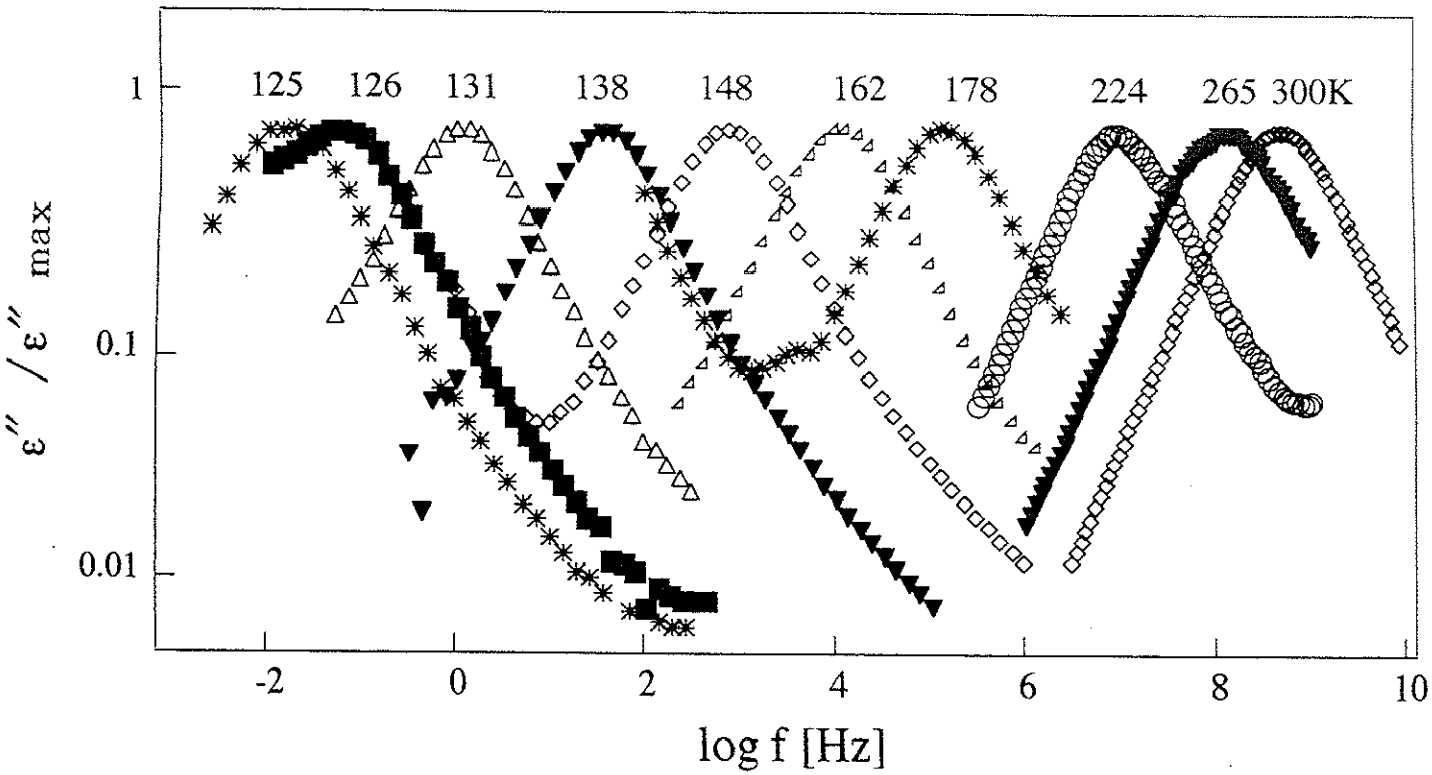

Fig. 4. 1 Spectra of i-propanol at various temperatures. The number above each spectrum represents the measuredment temperature.

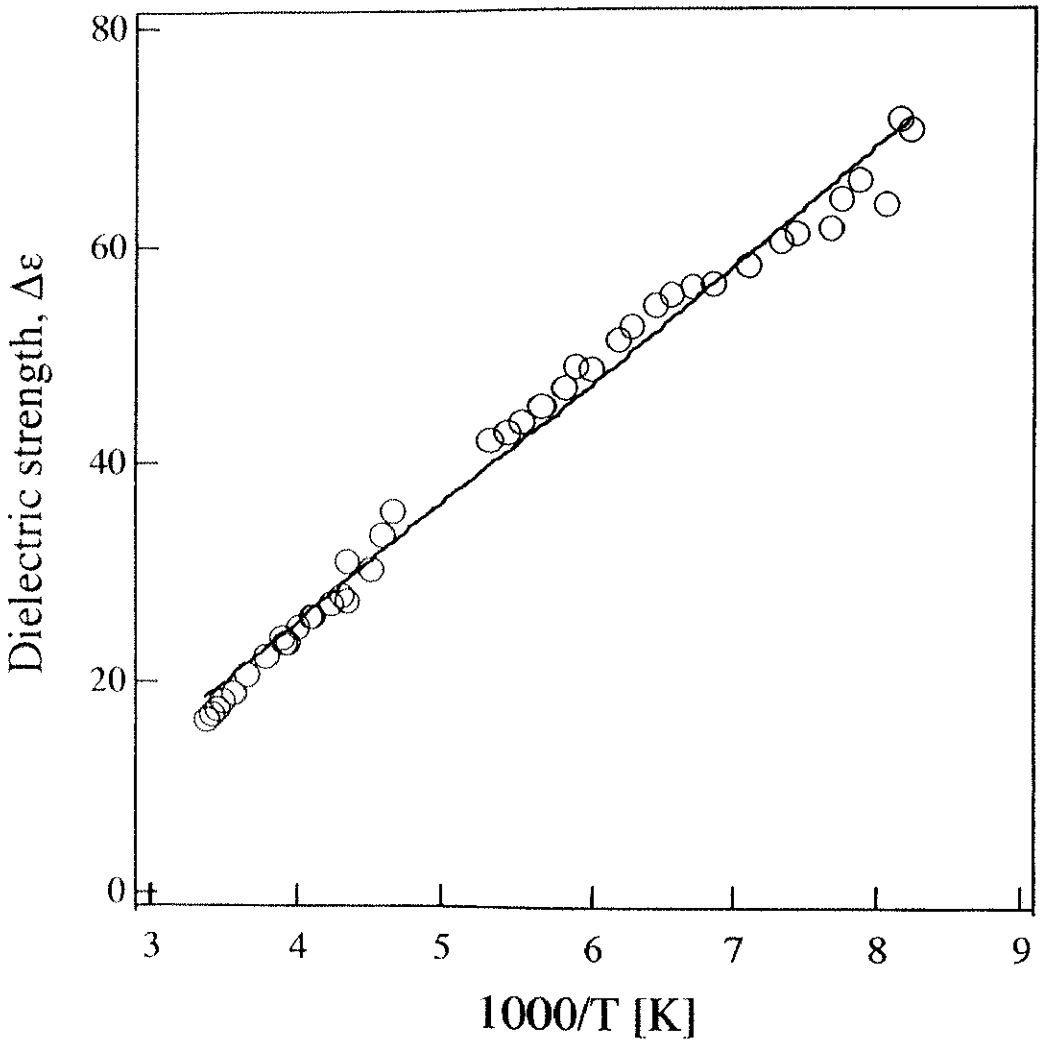

Fig. 4. 2 Temperature dependence of the dielectric strength for i-propanol. $\Delta\varepsilon(T)$ can be well described by the modified Onsager equation, $\Delta\varepsilon = -10.9 + 18.1 \times 10^3/T$.

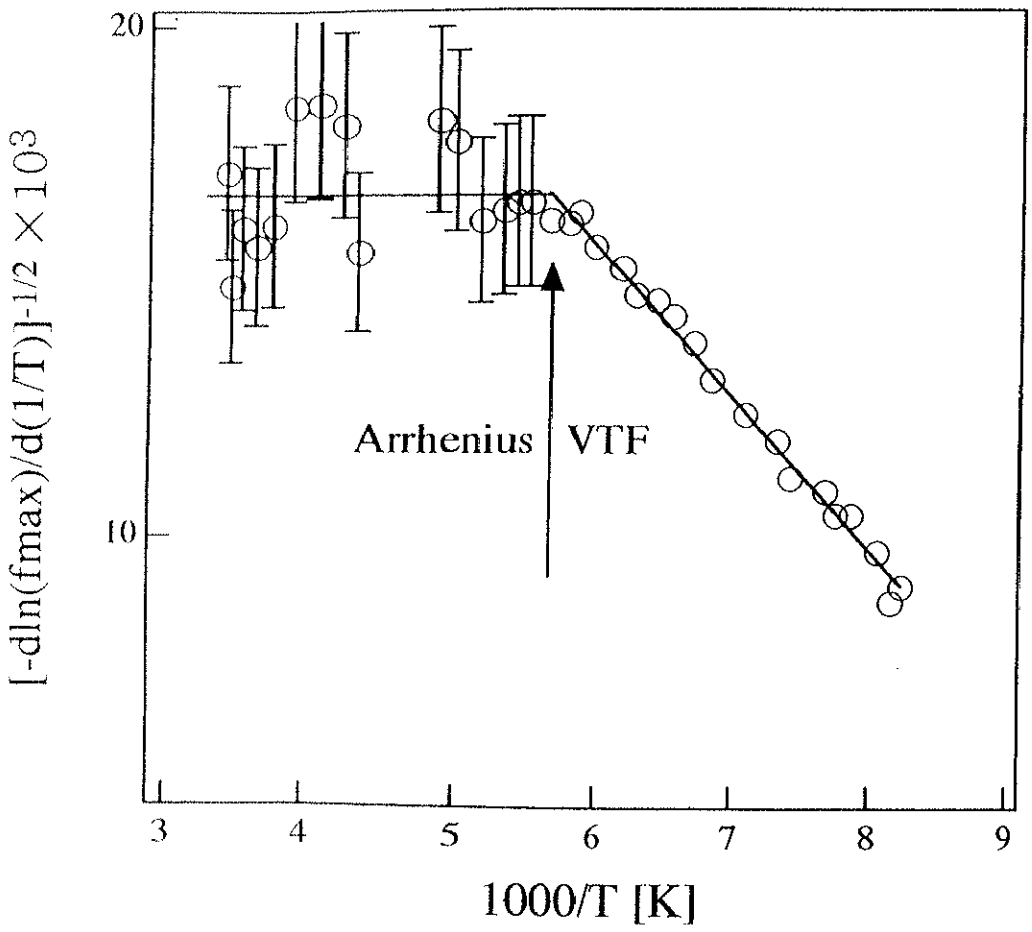

Fig. 4. 3 An example of temperature derivative analysis for i-propanol. The VTF expression can be linearized in the low temperature range and the Arrhenius expression appears as a horizontal line in the high temperature range.

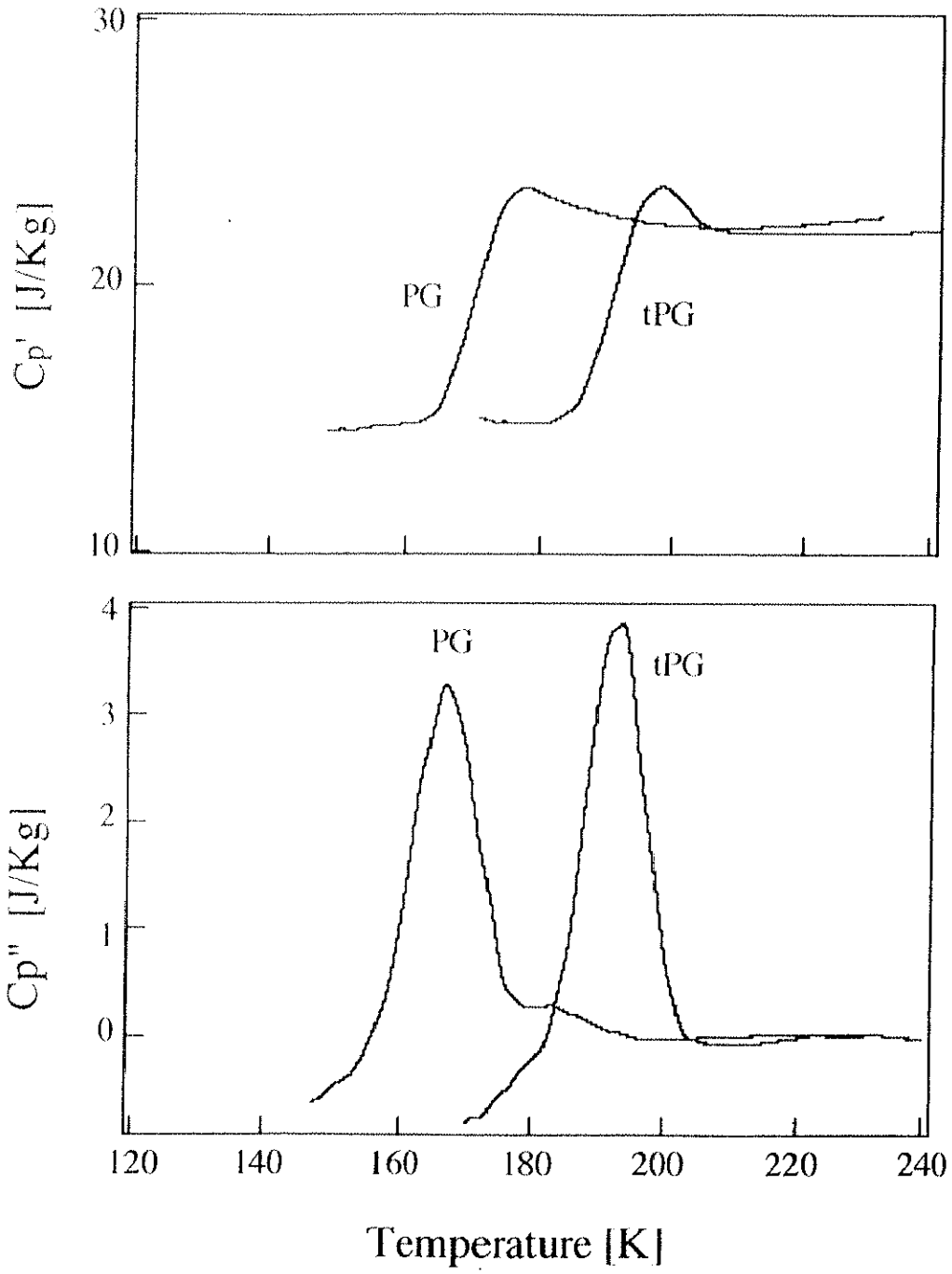

Fig. 4. 4 The typical a) real and b) imaginary parts of complex heat capacity $C_p^*(T) = C_p'(T) - i\, C_p''(T)$ for Propylene Glycol (PG) and tri Propylene Glycol (tPG).

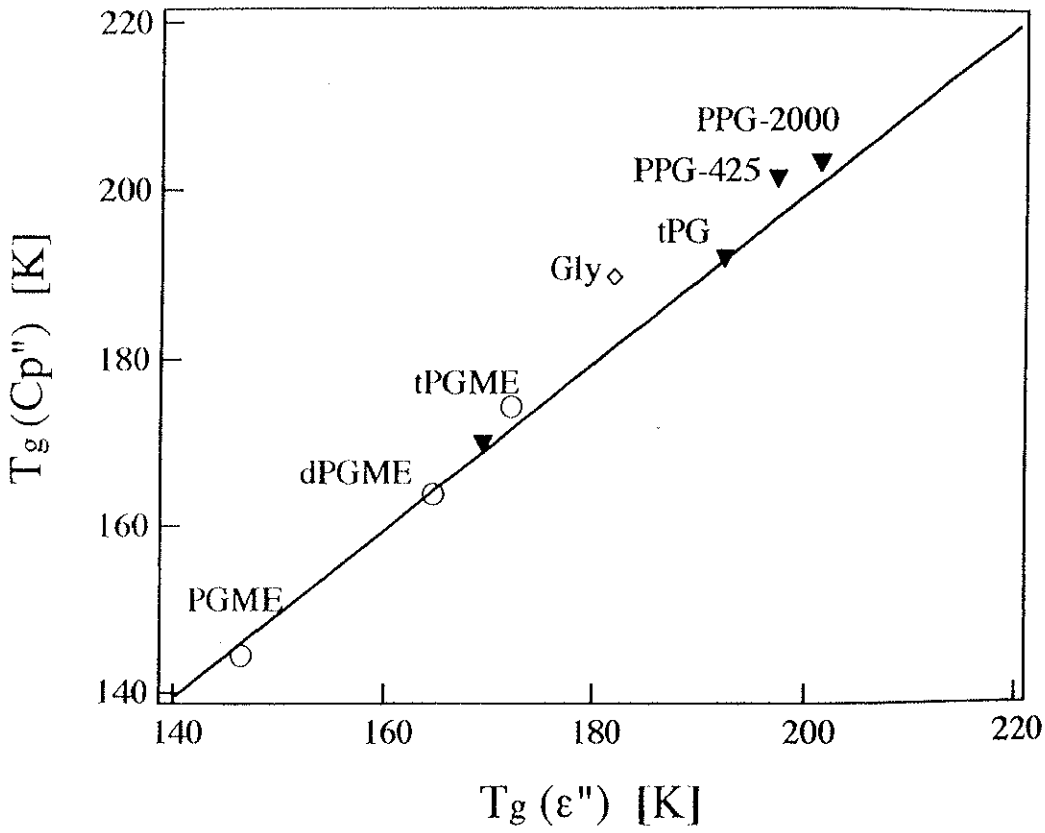

Fig. 4. 5 Relationship between the calorimetric $T_g(C_p")$ and dielectric $T_g(\varepsilon")$. The peak of $C_p"$ is defined as $T_g(C_p")$. $T_g(\varepsilon")$ is the temperature where the relaxation time is 100 sec. Two glass transitions temperatures are in agreement within experimental uncertainty.

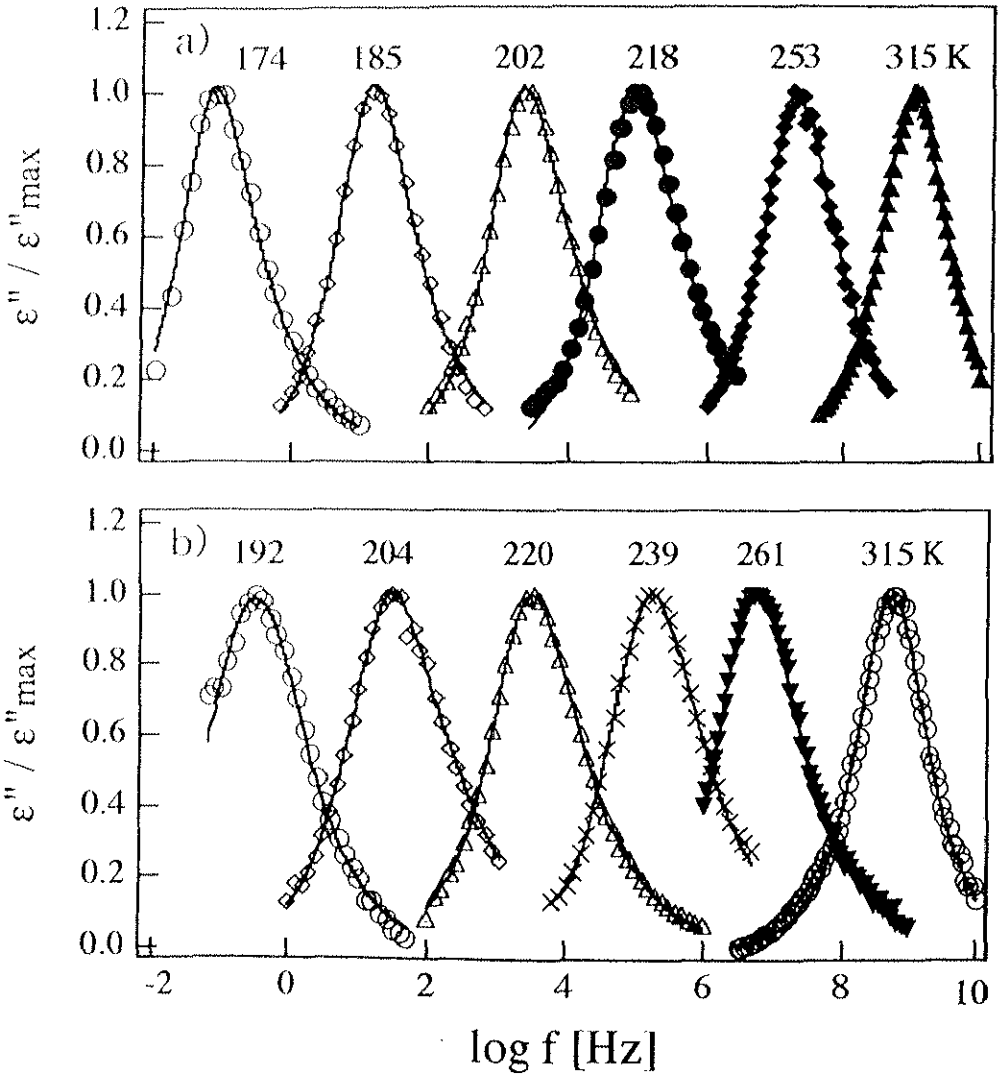

Fig. 5. 1 Normalized dielectric loss curves, $\varepsilon''/\varepsilon''_{max}$, of a) Propylene Glycol and b) Glycerol at several fixed temperatures. The solid lines are fits by the Havriliak-Negami function.

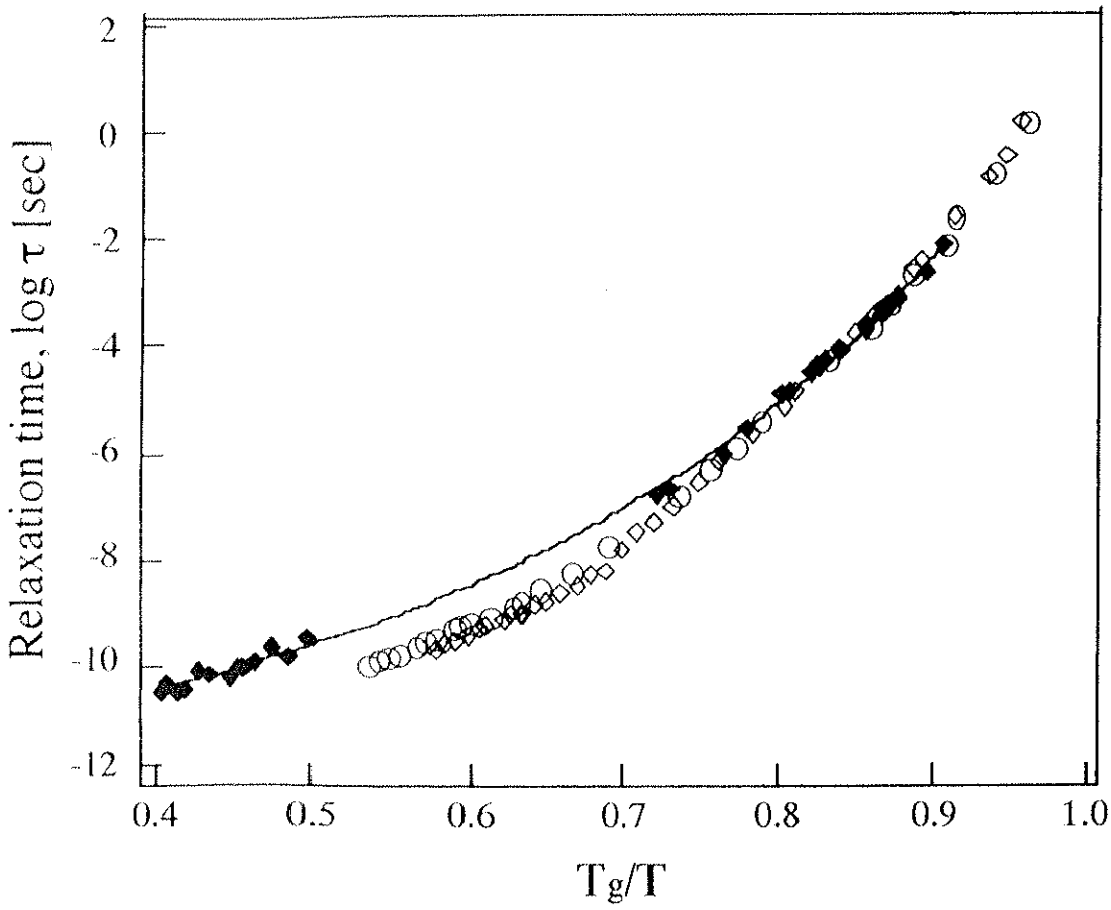

Fig. 5. 2 Angell's representation for n-Propanol (◆), Propylene Glycol (○) and Glycerol (◇). The solid line is a guide for the eye. T_g is the glass transition temperature at which the relaxation time is 100 sec.

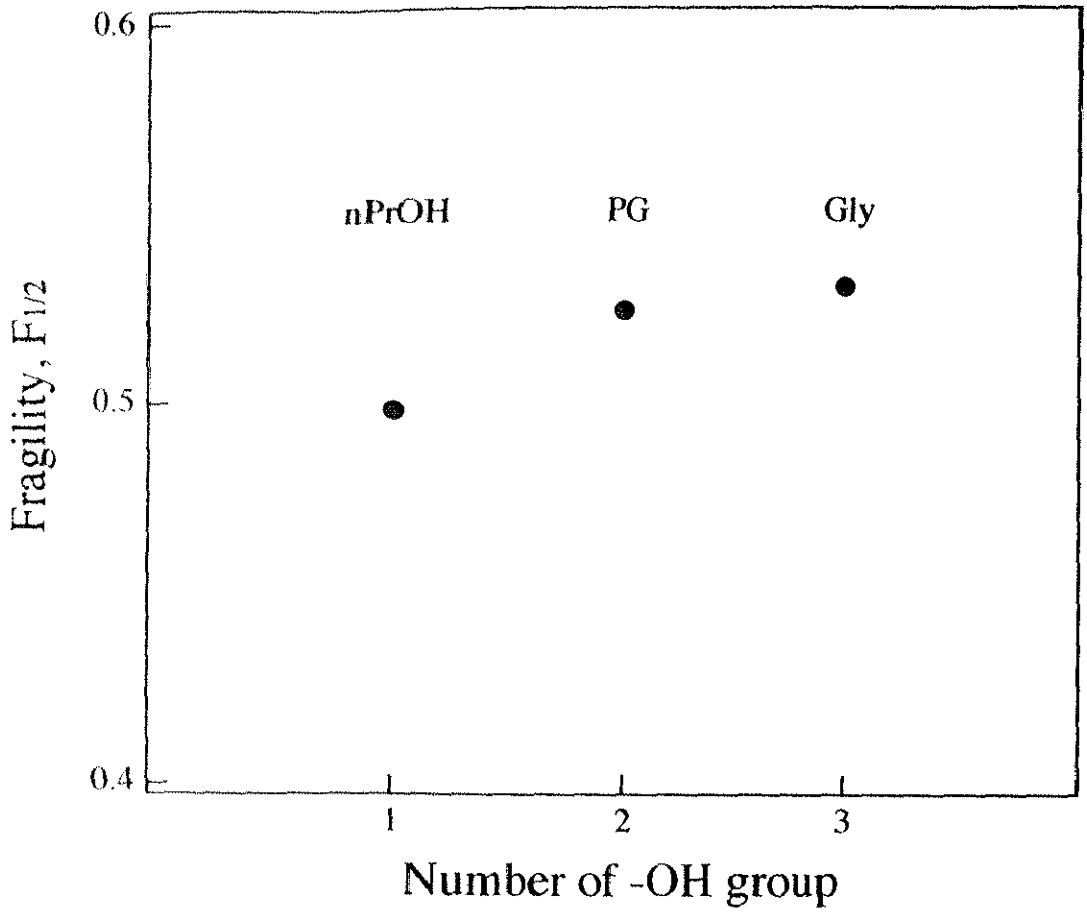

Fig. 5. 3 Fragility, $F_{1/2}$, for n-Propanol (nPrOH), Propylene Glycol (PG) and Glycerol (Gly).

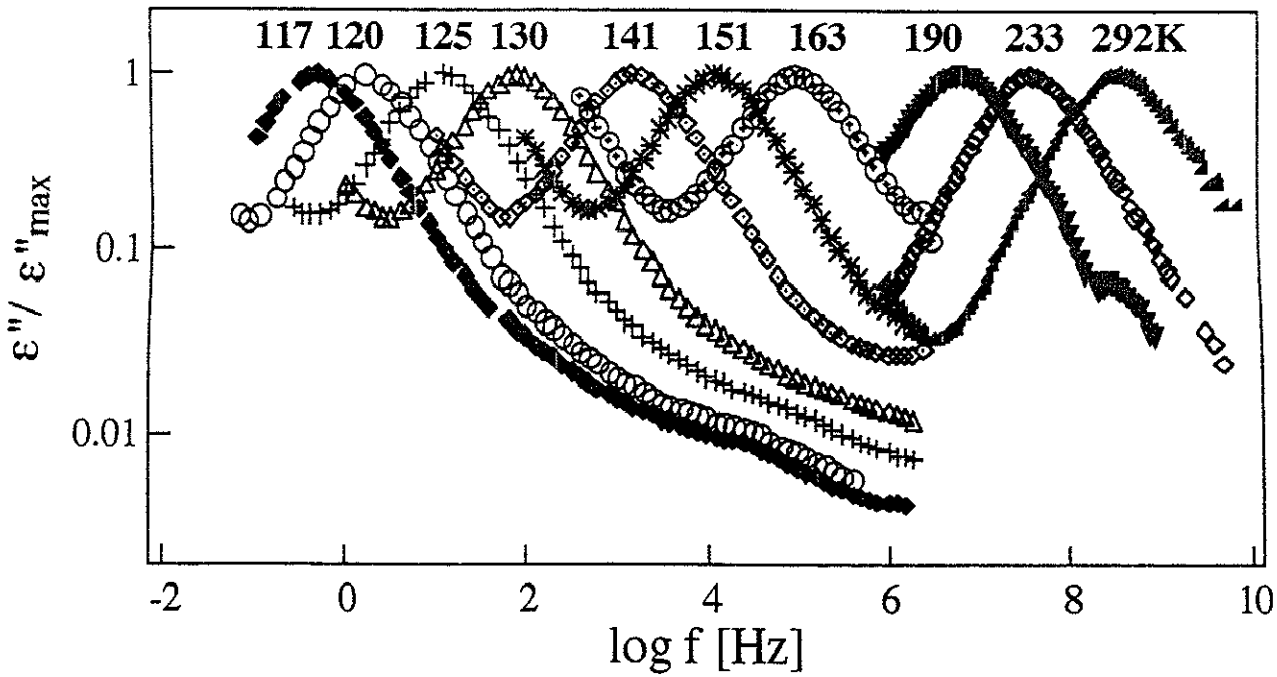

Fig. 5. 4 Spectra of n-propanol at various temperatures. The number above each spectrum represents the measurement temperature.

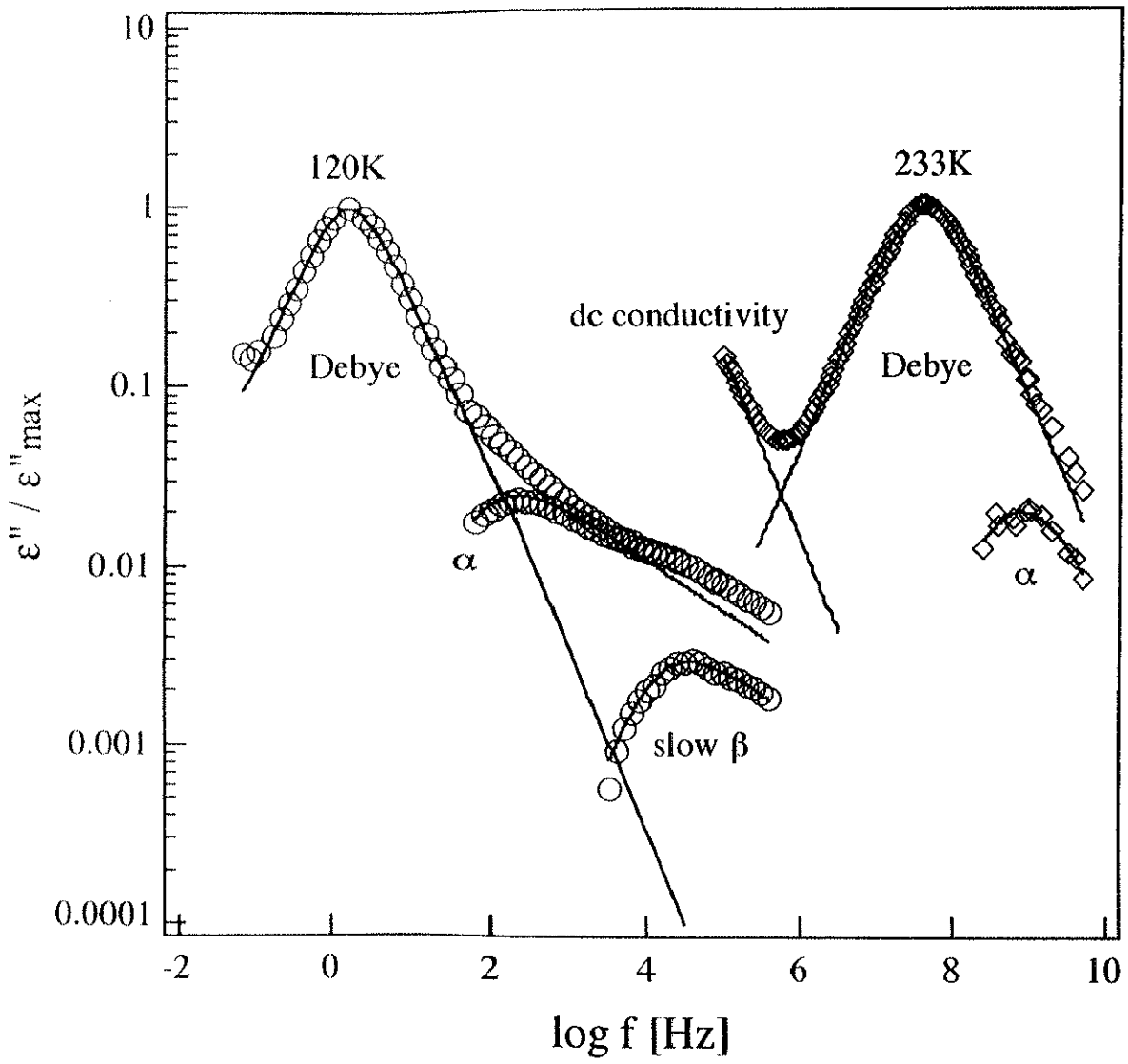

Fig. 5. 5 Three relaxation modes for n-Propanol. Three relaxation processes were named Debye, α and slow β relaxations. The Debye relaxation shows the Debye-type frequency dependence. The α and slow β relaxations were reproduced by the Havriliak-Negami function.

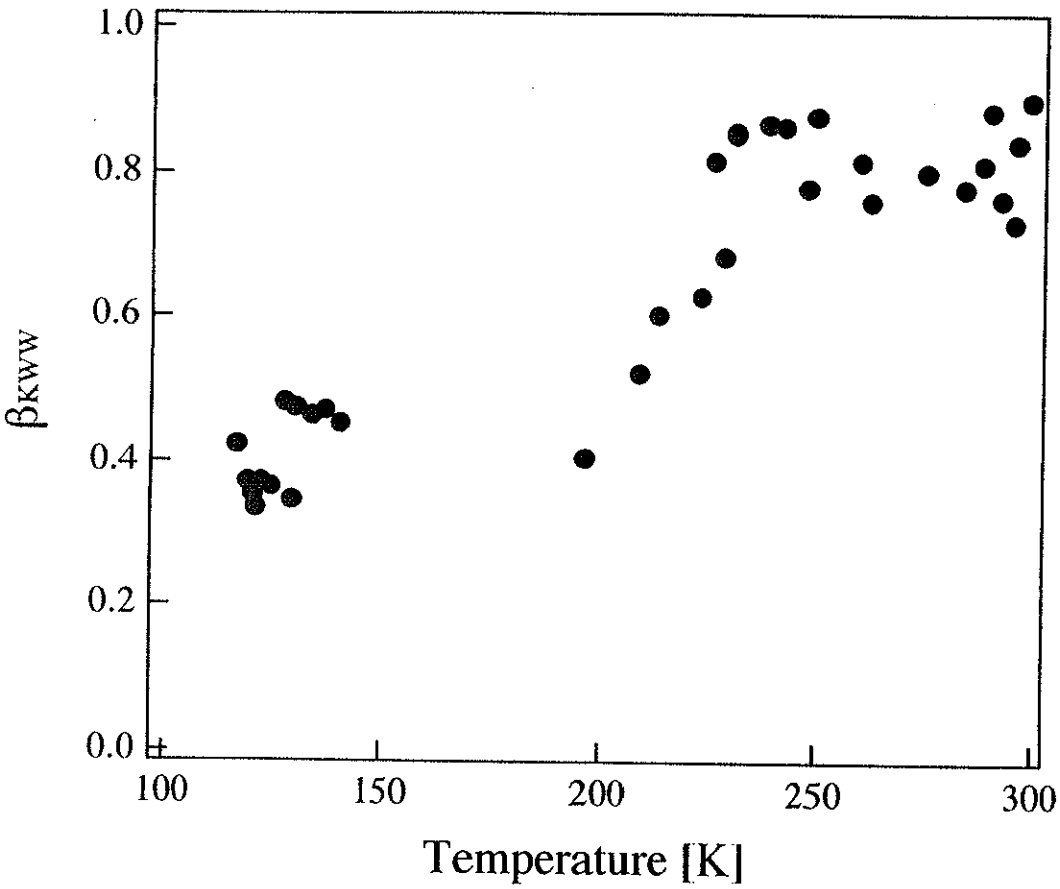

Fig. 5. 6 Temperature dependence of β_{KWW} for the α relaxation of n-Propanol. It seems that β_{KWW} increases monotonically with increasing temperature.

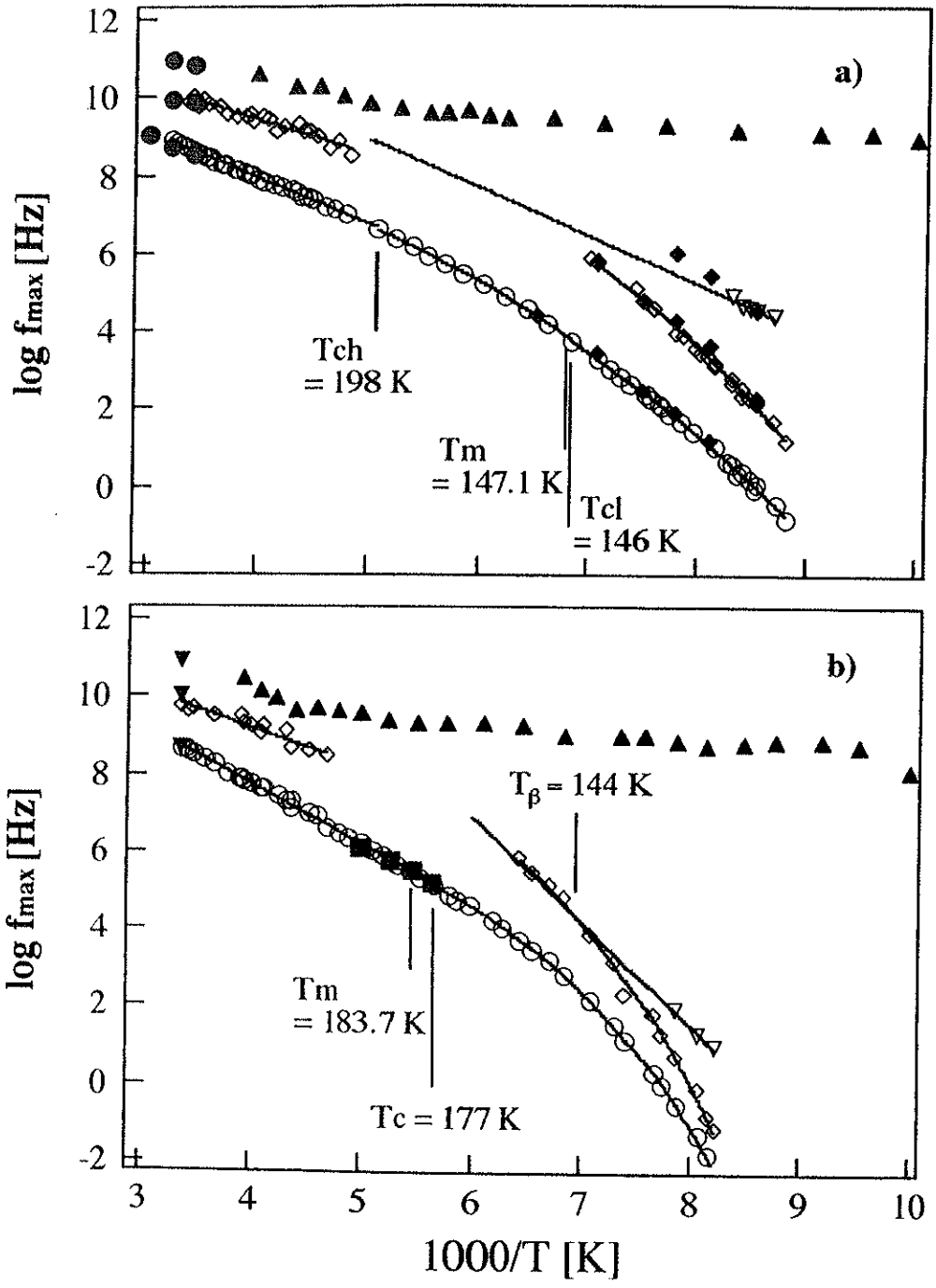

Fig. 5. 7 Temperature dependence of the dielectric relaxation frequency for three relaxation modes in a) n-Propanol and b) i-Propanol, respectively. The marks ○, ◇ and ▽ mean Debye, α and slow β relaxations, respectively. The dielectric relaxation frequency reported already for n-Propanol {[53] (◆) and [54] (●)} and i-Propanol {[64] (▼), [65] (■)} are plotted together for comparison. The relaxation frequency determined by Brillouin scattering [66] (▲) are drawn together. T_m means the melting temperature. There are crossover temperatures T_{ch} and T_{cl} for n-Propanol and T_c for i-Propanol.

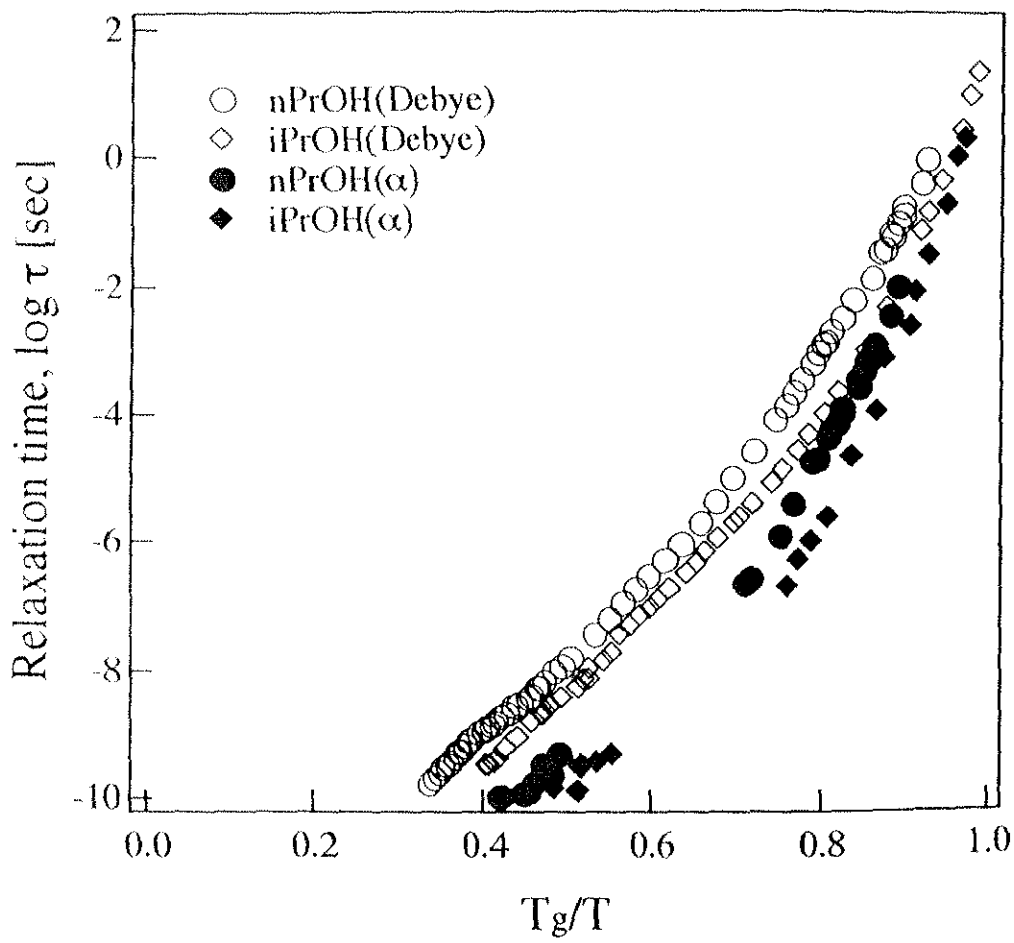

Fig. 5. 8 Relaxation time of the Debye and α relaxation processes for n-Propanol (nPrOH) and i-Propanol (iPrOH) vs. T_g/T. It is clearly seen that nPrOH is stronger than iPrOH.

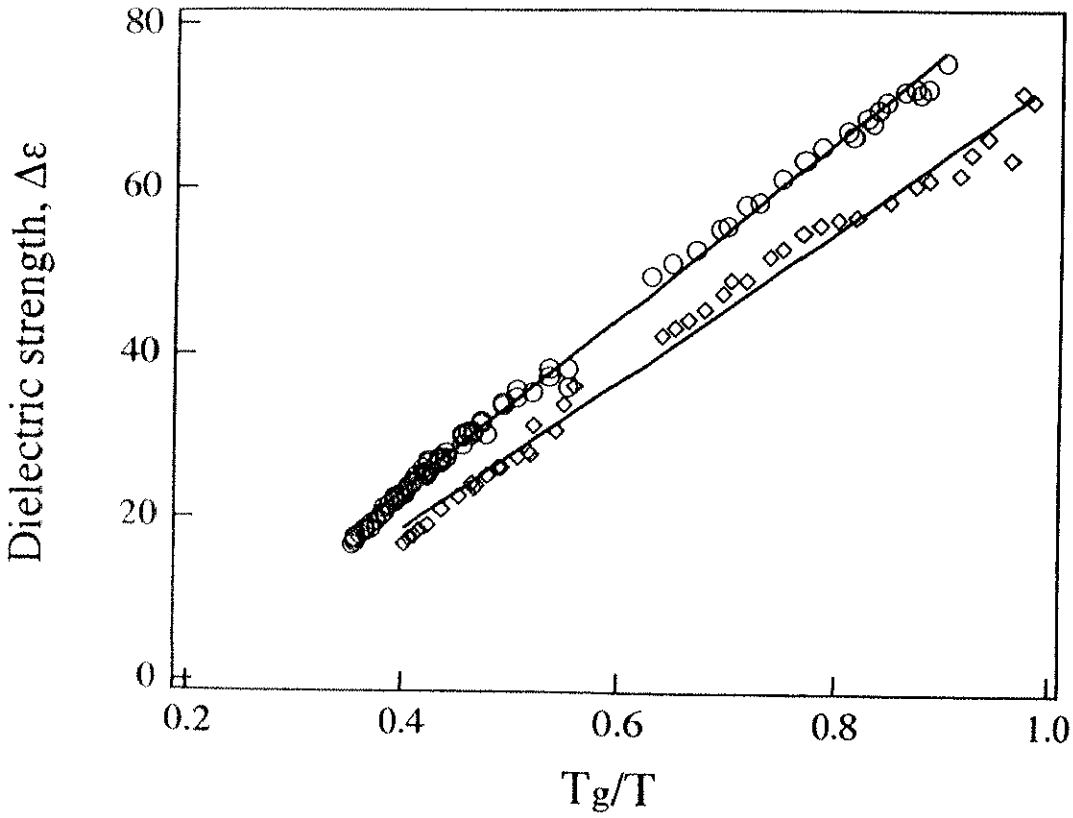

Fig. 5. 9 Dielectric strength vs Tg/T of both n-Propanol (○) and i-Propanol(◇)

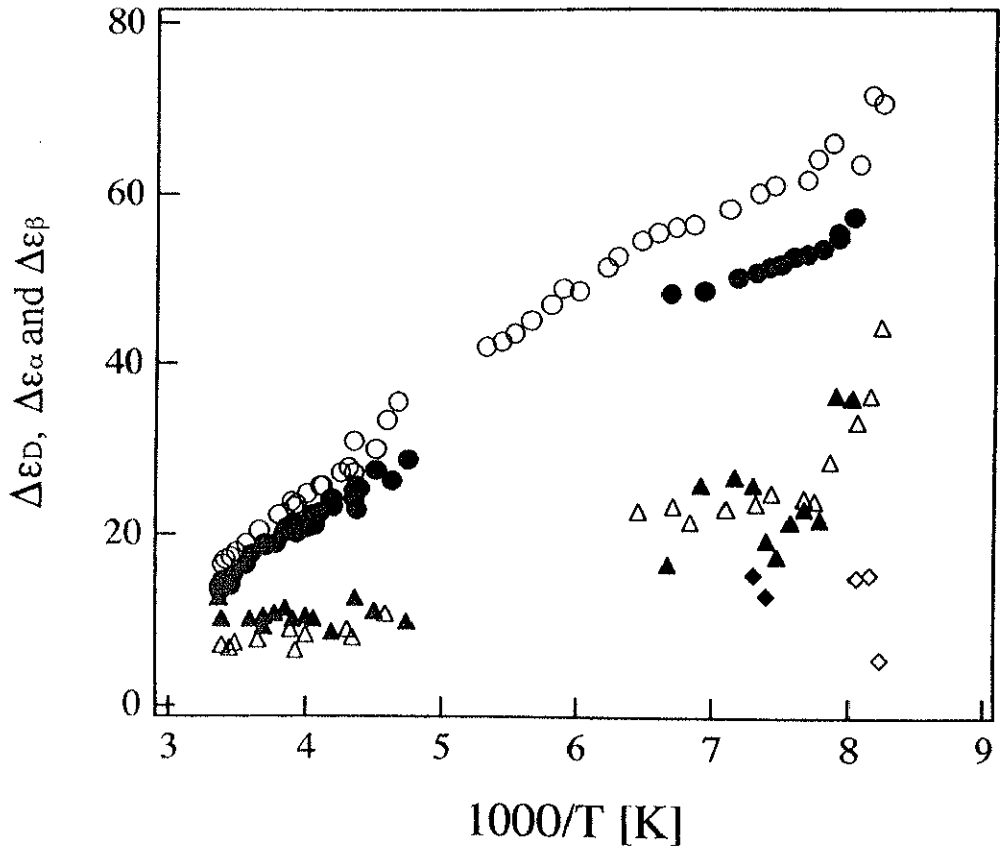

Fig. 5. 10 Temperature dependence of the dielectric strengths or i-Propanol (open) and i-Propanol-d1 (filled). Expect the case of Debye relaxation, $\Delta\varepsilon_D(T)$ (○ and ●), the values of α, $\Delta\varepsilon_\alpha(T)$) (△ and ▲), and slow β relaxation, ($\Delta\varepsilon_\beta(T)$) (◇ and ◆), are 10 and 50 times of the raw data, respectively.

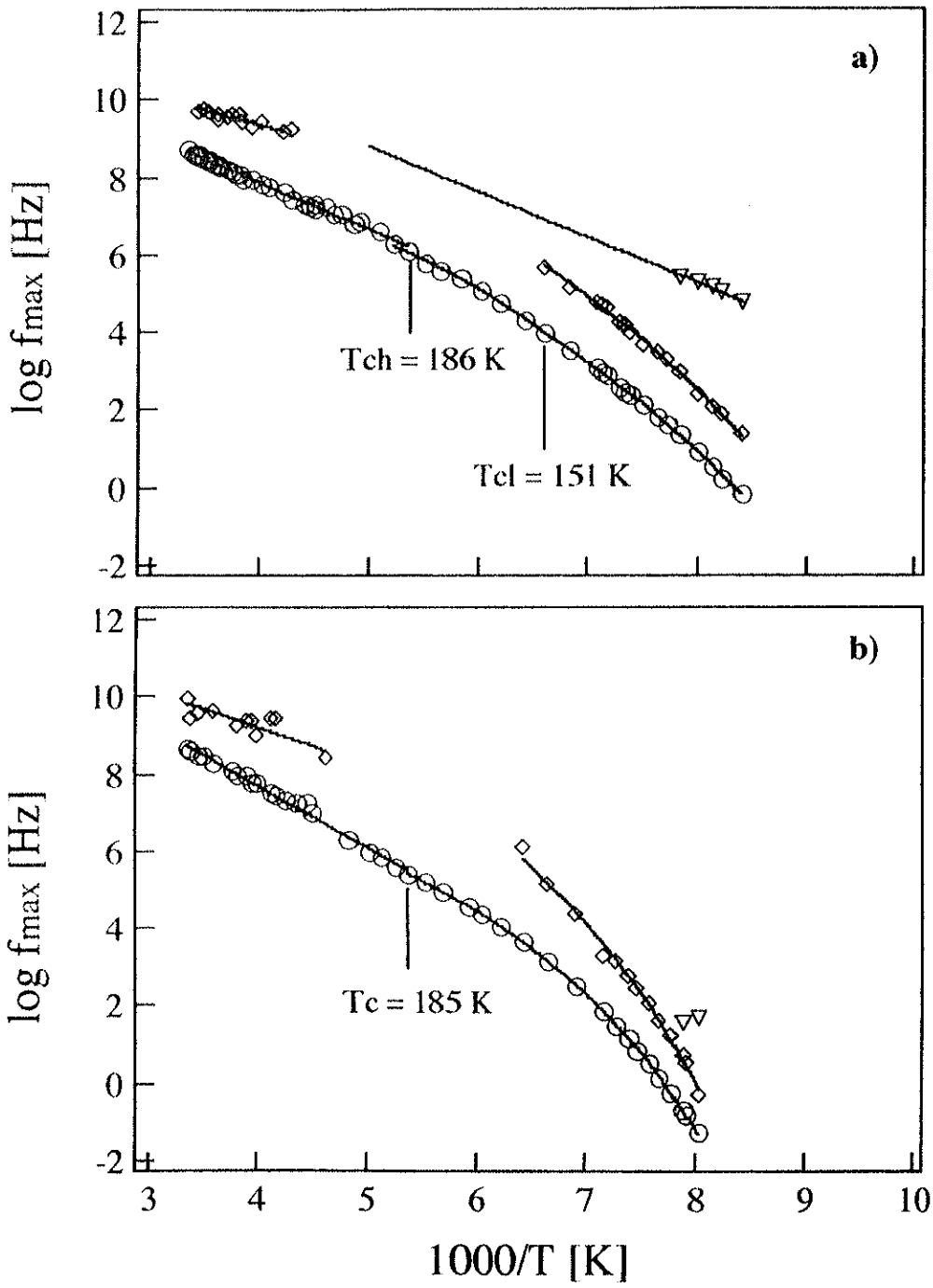

Fig. 5. 11 Temperature dependence of the dielectric relaxation frequency for three relaxation modes in a) n-Propanol-d1 and b) i-Propanol-d1, respectively. The marks ○, ◇ and ▽ mean the Debye, α and slow β relaxations, respectively. The solid lines are the best fits.

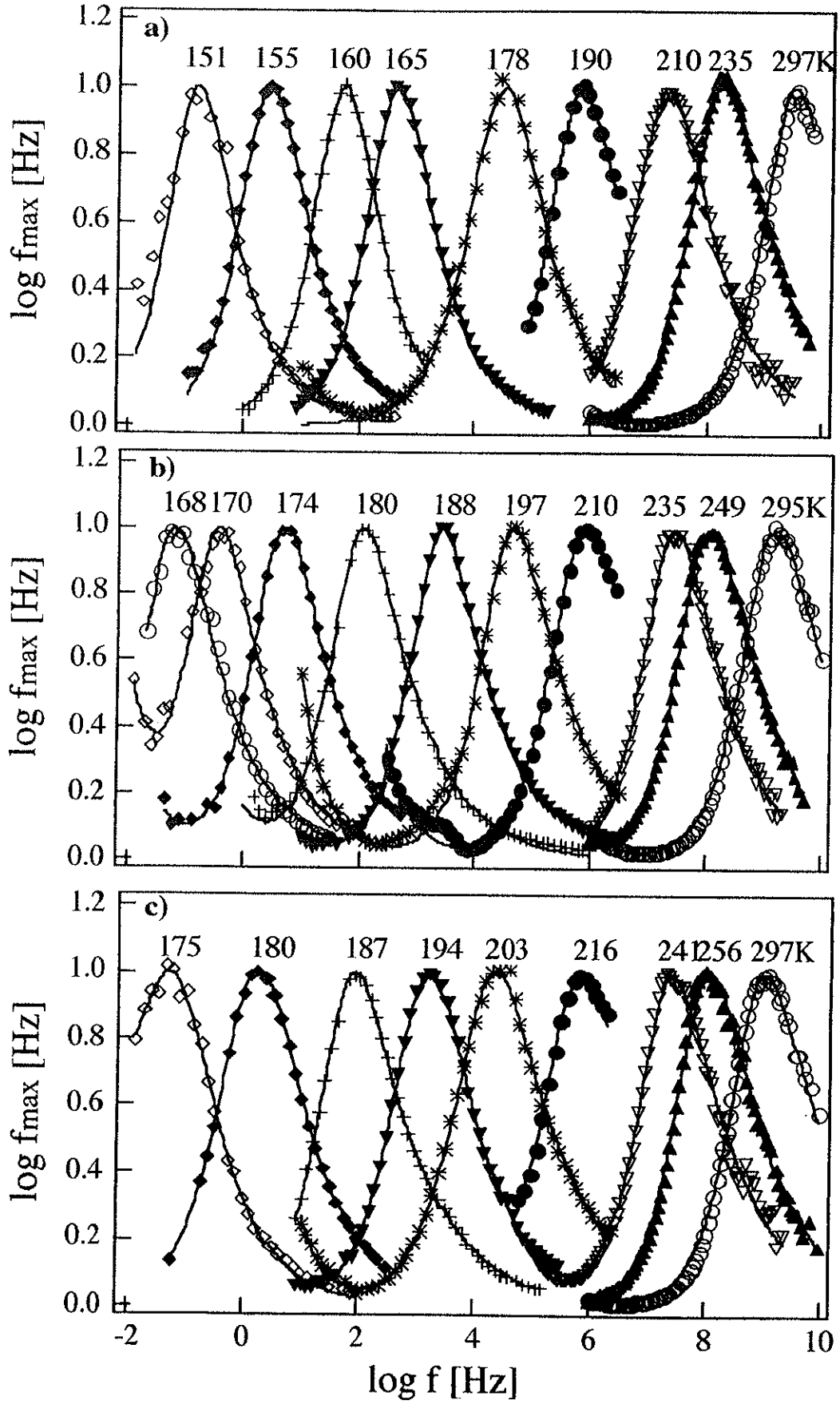

Fig. 5. 12 Normalized dielectric loss curves, $\varepsilon''/\varepsilon''_{max}$, of a) PGME, b) dPGME and c) tPGME at several fixed temperatures. The solid lines are the fits by the Havriliak-Negami function. Only the main relaxation mode was extracted from the spectra.

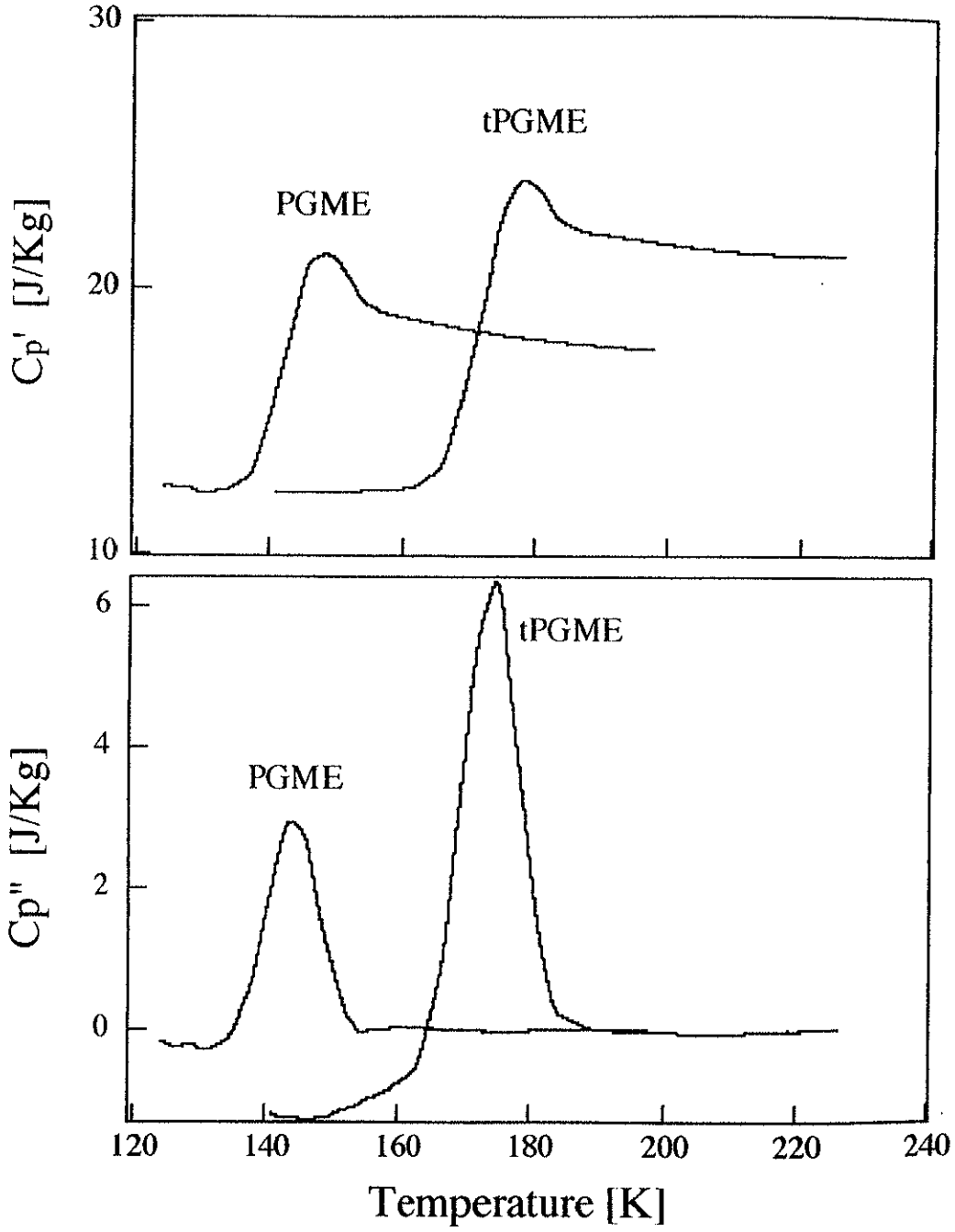

Fig. 5. 13 The typical a) real and b) imaginary schemes of complex heat capacity $C_p^*(T) = C_p'(T) - i\, C_p''(T)$ for PGME and tPGME.

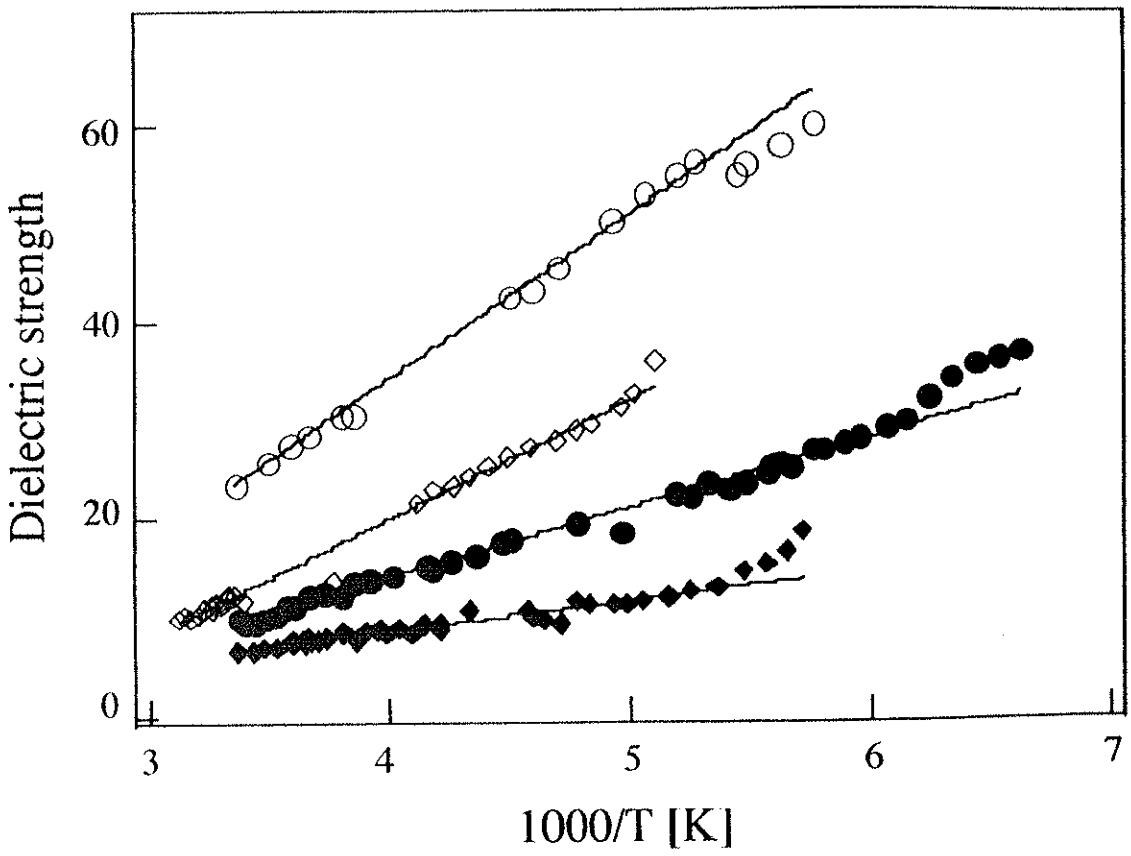

Fig. 5. 14 Dielectric strength of PG (○), tPG (◇), PGME (●) and tPGME (◆). Solid lines are the best fits.

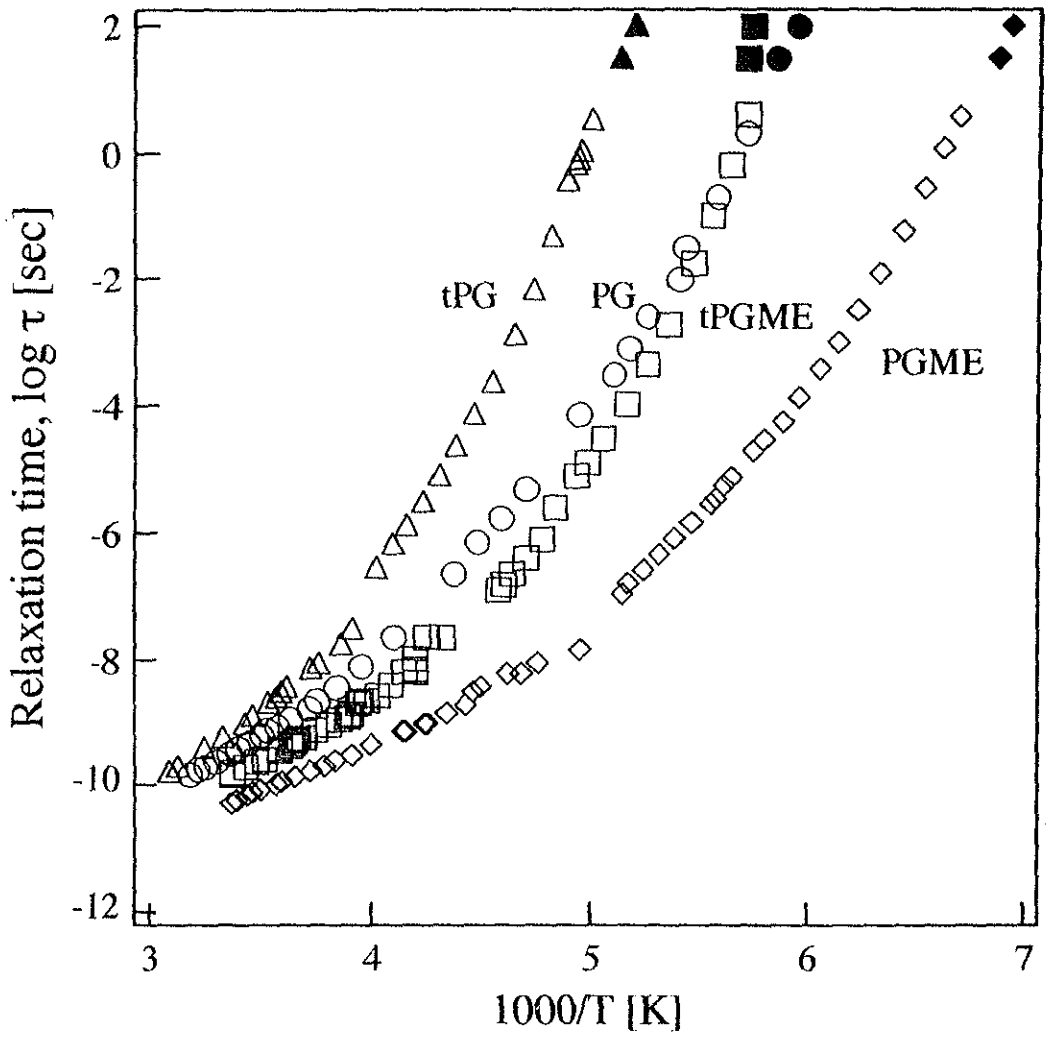

Fig. 5. 15 Dielectric relaxation time (τ) for PG (○), tPG (△), PGME (◇) and tPGME (□) and the their corresponding calorimetric relaxation time for PG (●), tPG (▲), PGME (◆) and tPGME (■)

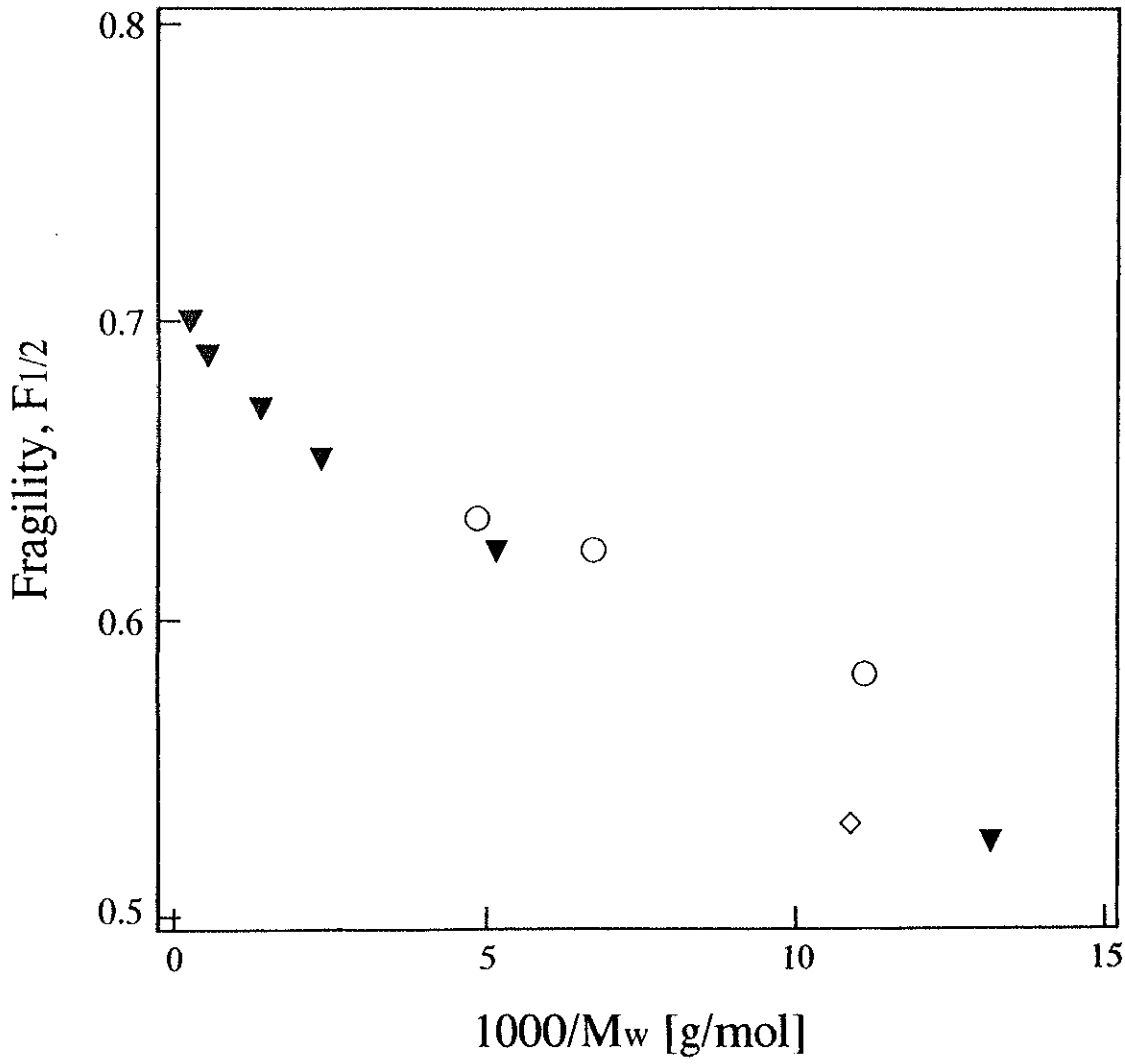

Fig. 5. 16 Relationship between the fragility, $F_{1/2}$, and molecular weight, M_w, for PGME (○) and PG (▼) families and Gly (◇). The samples are listed at Table 5. 6

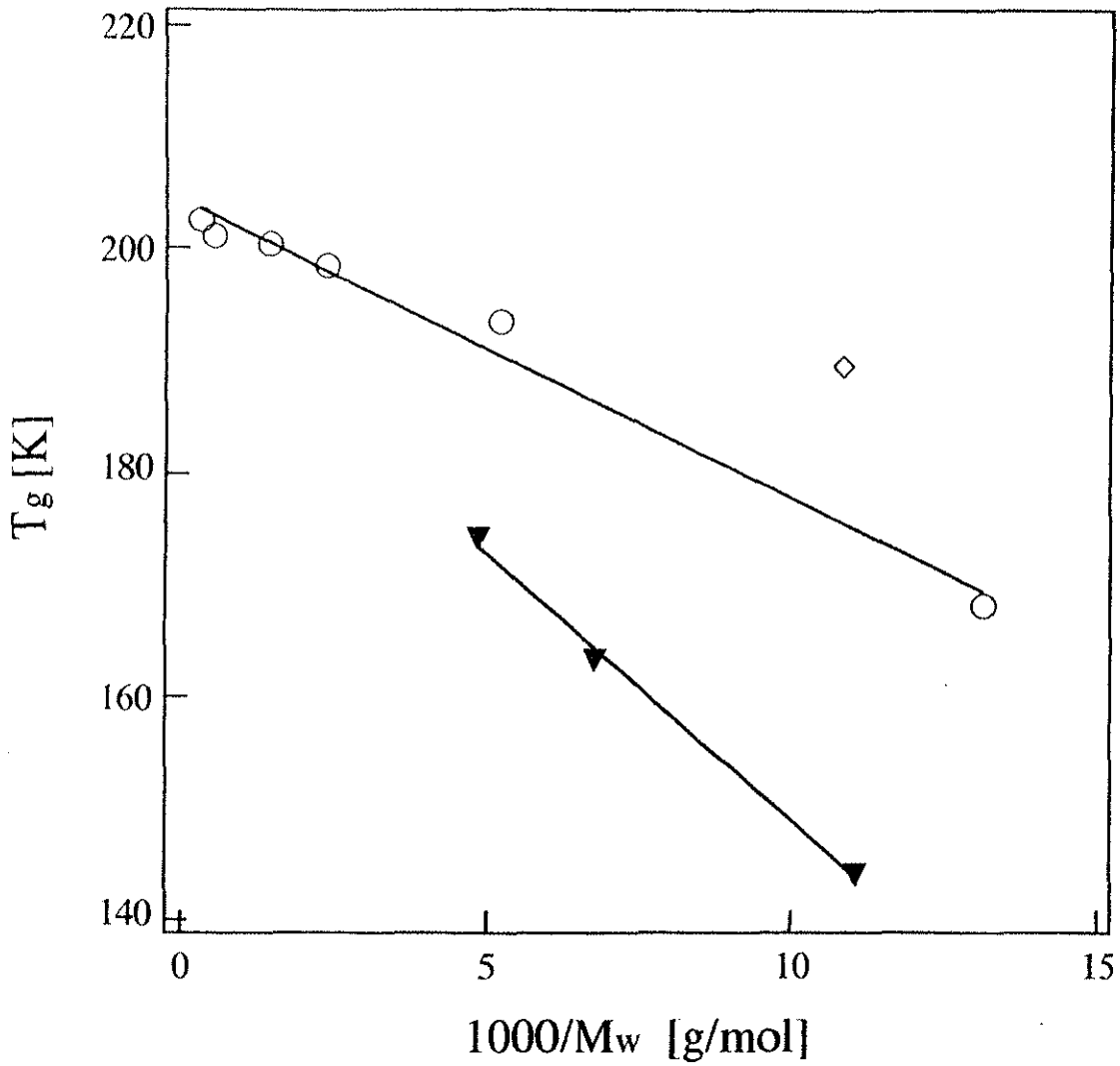

Fig. 5. 17 Relationship between the glass transition temperature, T_g, and molecular weight, Mw for PGME (○) and PG (▼) families and Gly (◇). The samples are listed at Table 5. 6. The solid lines are the best fits of $Tg \propto -1/Mw$

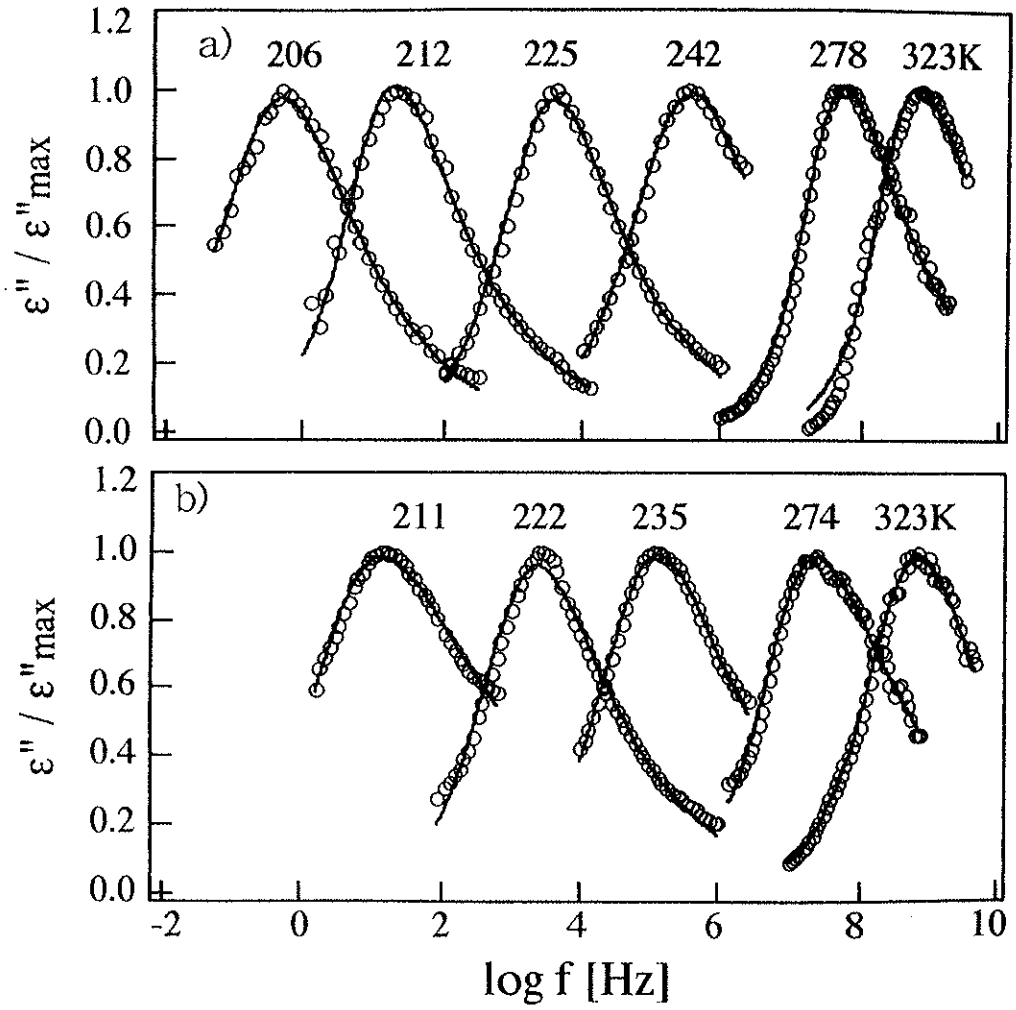

Fig. 5. 18 Normalized dielectric loss spectra, ε"/ ε"max, of a) tPG and b) PPG-4000 at several fixed temperatures. The solid lines are fits by the Havriliak-Negami function.

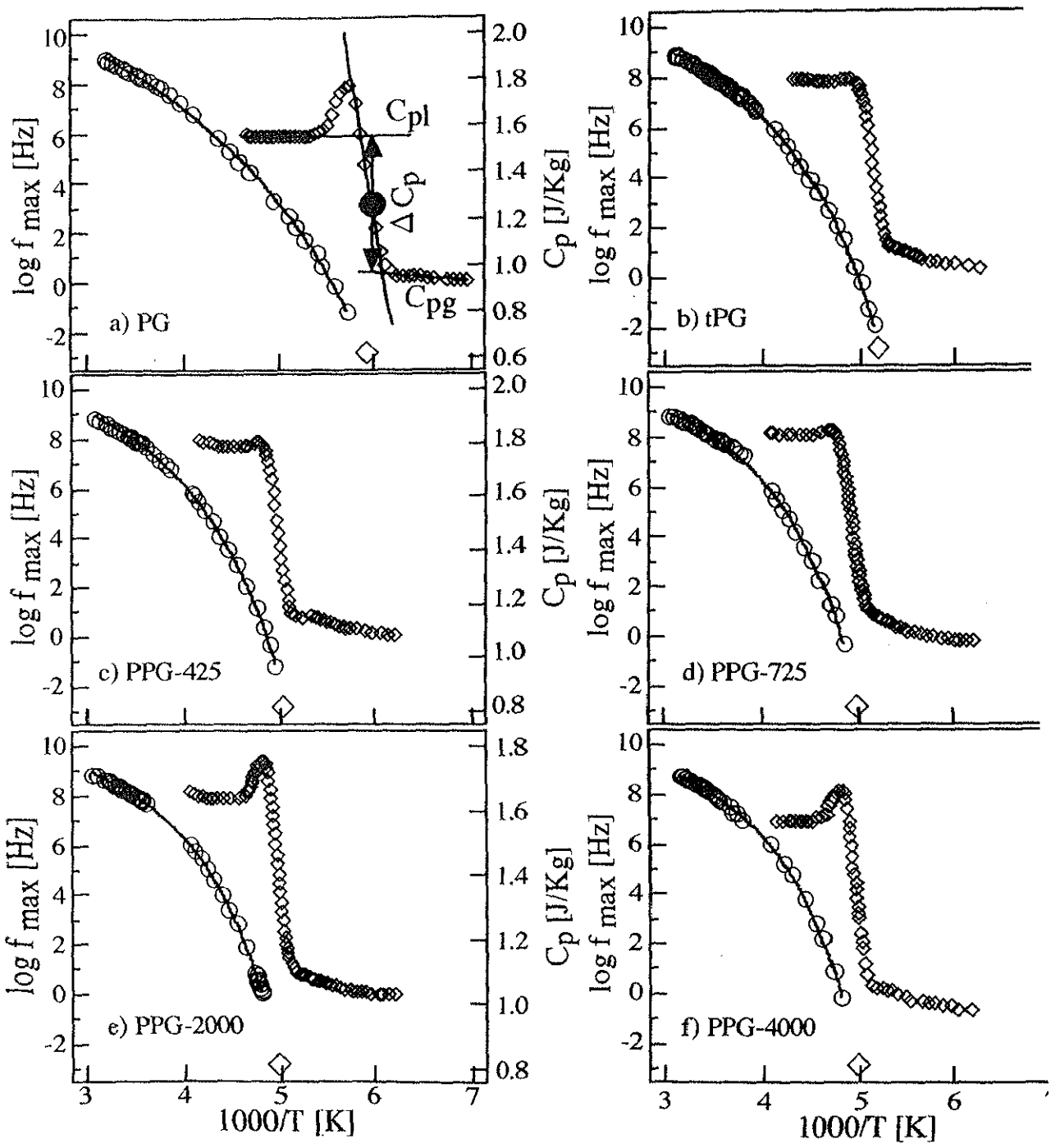

Fig. 5. 19 Relaxation frequency f_{max} the dielectric loss and heat capacity C_p' at constant pressure vs. the inverse temperature for a) PG, b) tPG, c) PPG-425, d) PPG-725, e) PPG-2000 and f) PPG-4000. The solid lines in f_{max} frequency are the VTF fitted results. The ◇ and ● are the glass transition temperatures determined by dielectric and calorimetric measurements, respectively.

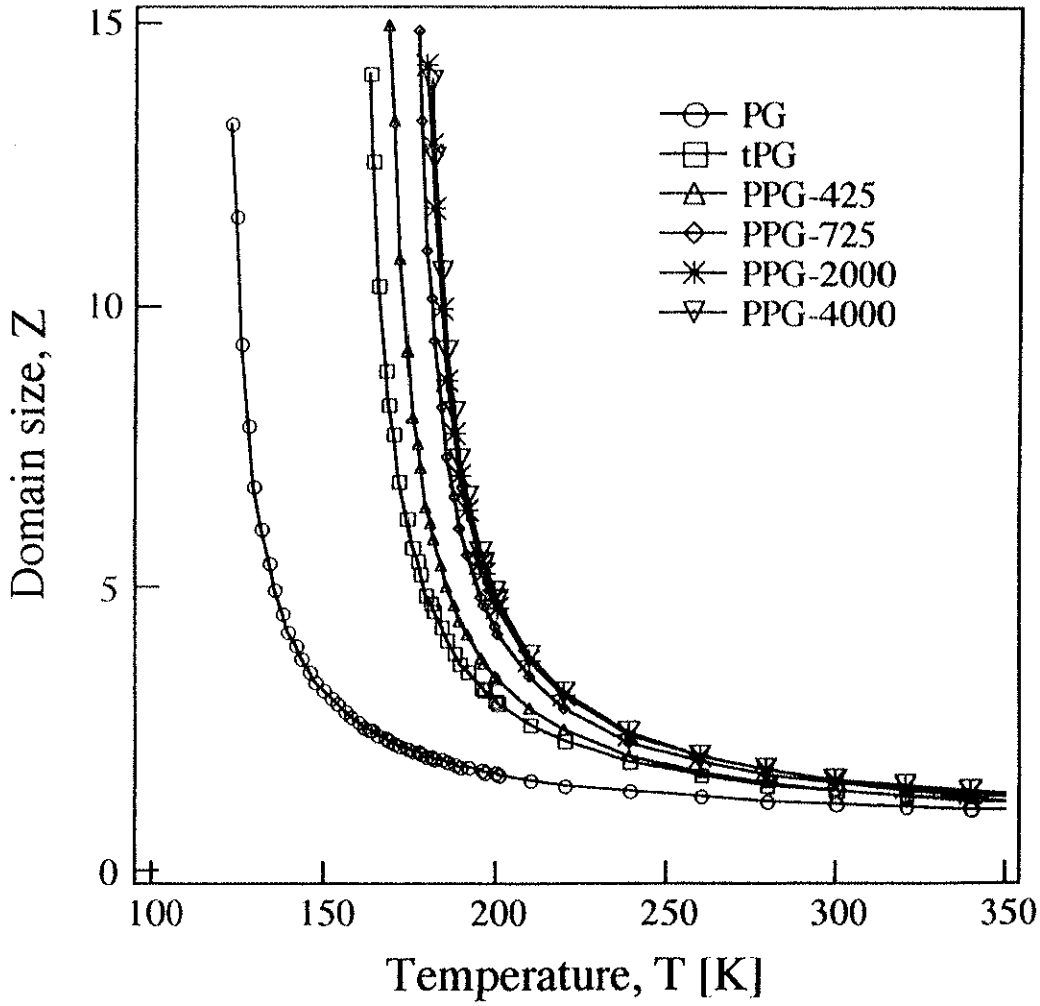

Fig. 5. 20 Temperature dependence of domain size, Z, for PG and PPGs.

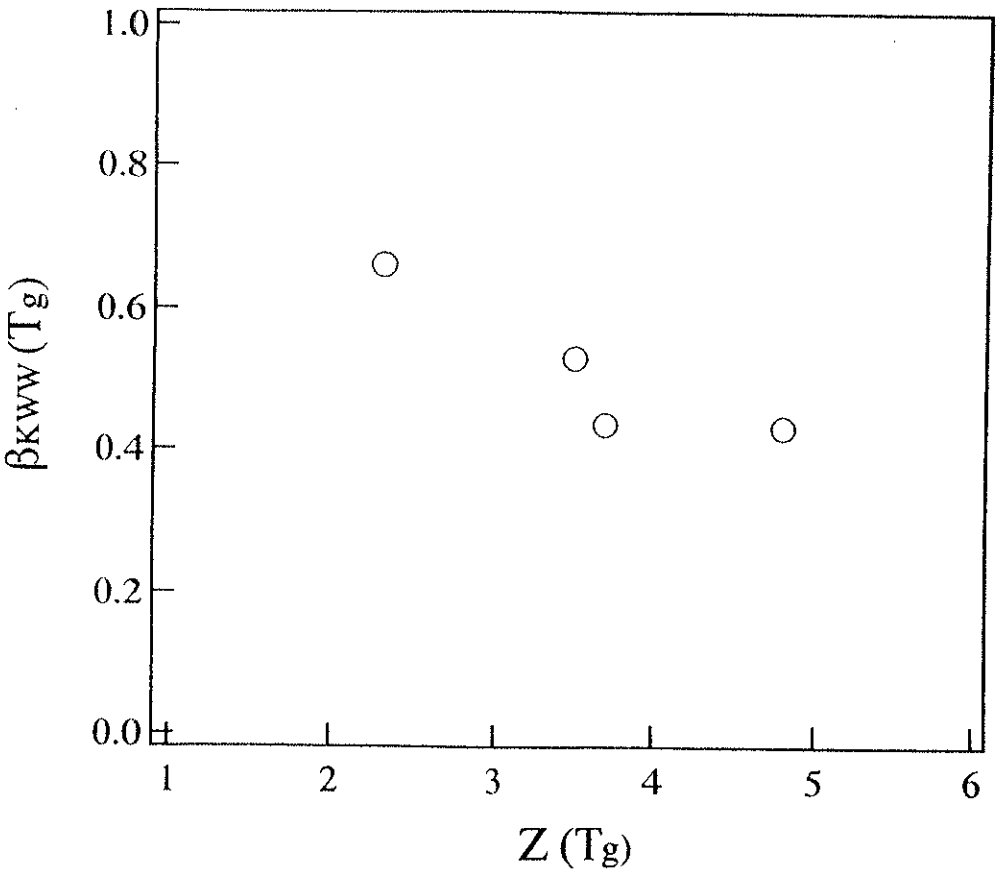

Fig. 5. 21 Relationship between the values for β_{KWW} in KWW function and the domain size Z at Tg, $\beta_{KWW}(T_g)$ vs $Z(T_g)$

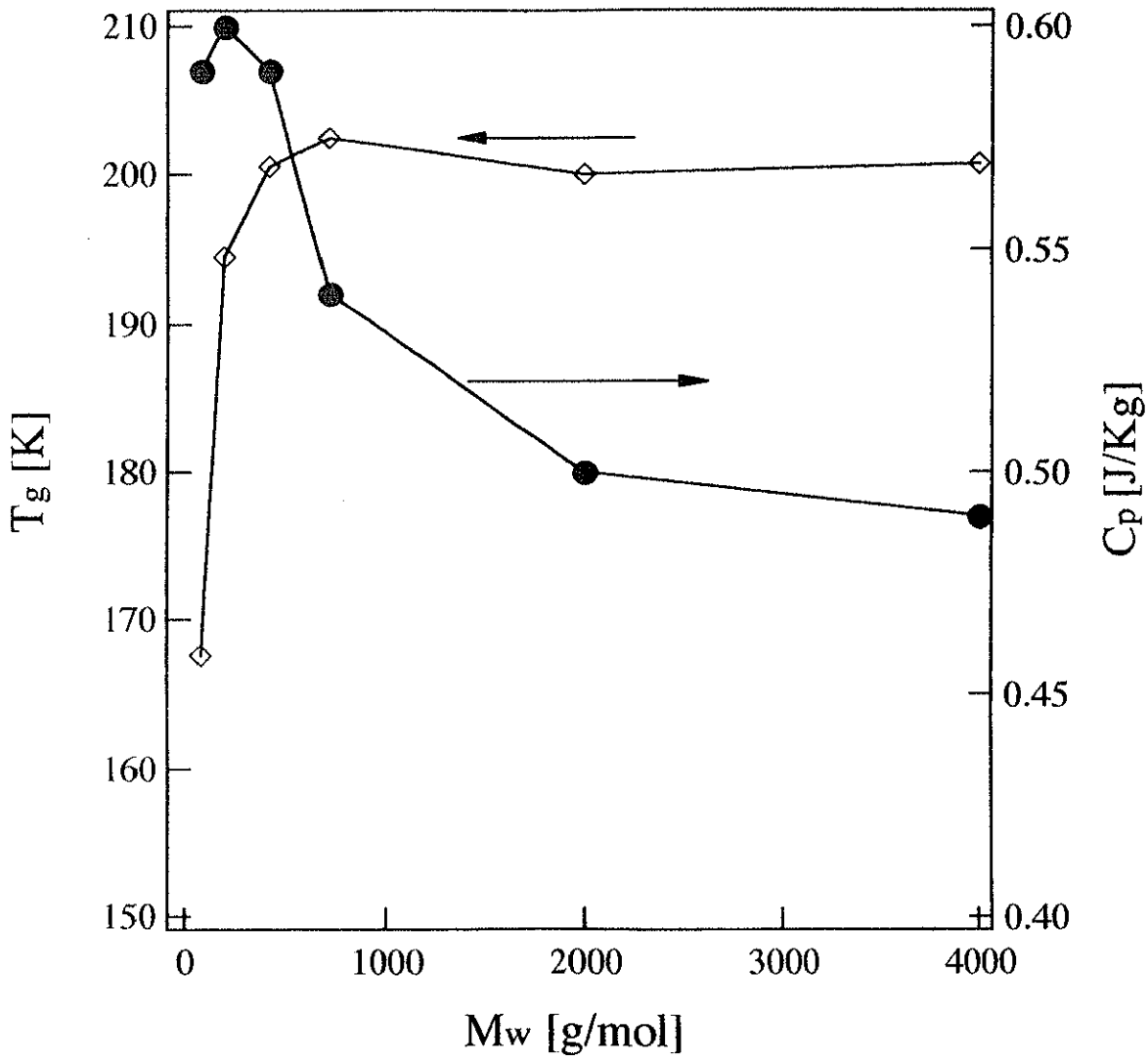

Fig. 5. 22 The calorimetric T_g (◇) and the heat capacity change $\Delta C_p(T_g)$ (●) are plotted against the molecular weight Mw.

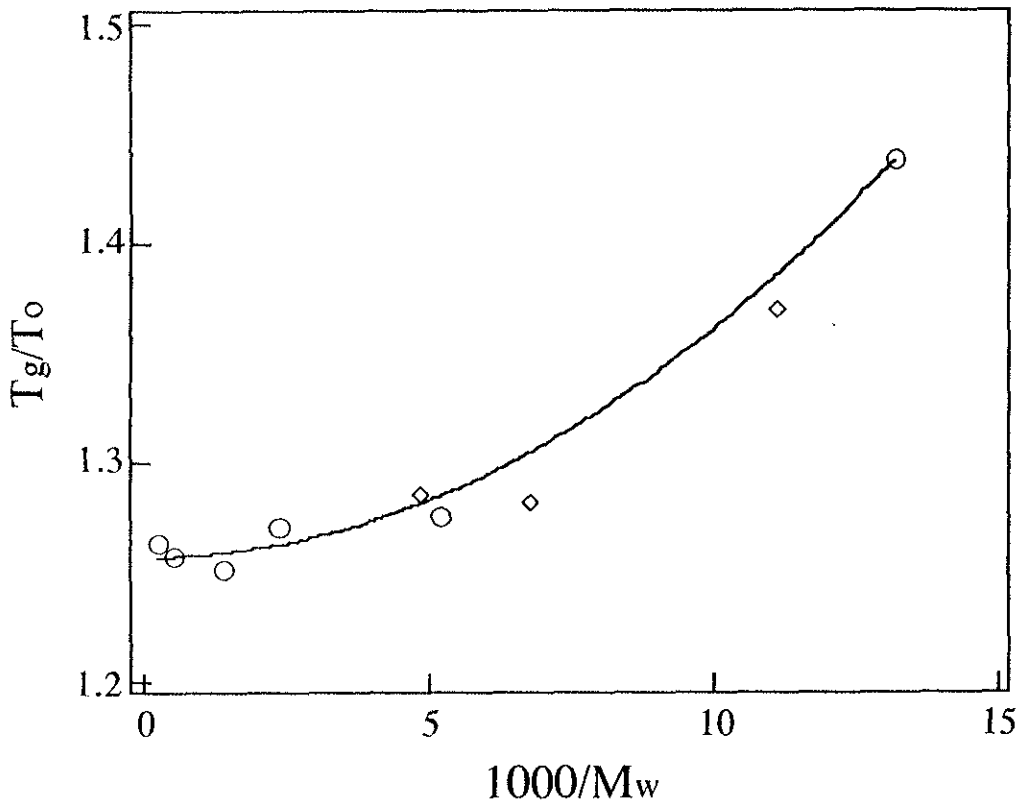

Fig. 5. 23 Molecular weight dependence of Tg/To for PG (○) and PGME families(◇).